Quaternary Science Reviews 343 (2024) 108929

Contents lists available at ScienceDirect

Quaternary Science Reviews

journal homepage: www.elsevier.com/locate/quascirev

# Massive Gulf of California diatom blooms mark silica boost from the Southern Ocean and intensification of El Niño and the North American monsoon in the transition to Greenland interstadial 12

Helen Griffin, Alan E.S. Kemp *, Richard B. Pearce

*School of Ocean and Earth Science, National Oceanography Centre, Southampton, University of Southampton, European Way, SO14 3ZH, UK*

ARTICLE INFO

Handling Editor: Dr I Hendy

ABSTRACT

Laminated sediments provide a rare opportunity to examine seasonal-scale ocean/atmosphere variation during abrupt climate transitions. Seasonal-scale changes through the transition from Heinrich Stadial 5 to Greenland Interstadial 12 are recorded in a sediment core (MD02-2515) from the Guaymas Basin, Gulf of California. The laminated sediments of the full interstadial have the highest opal concentrations (59.6 wt % biogenic silica) of the entire 55 kyr sequence and contain monospecific concentrations of the tropical oceanic diatom *Azpeitia nodulifera* that record flux from exceptional bloom events. Enhanced silica supply was likely initiated from the Southern Ocean during Heinrich Stadial 5, when Southern Hemisphere warming, via the bipolar seesaw mechanism, led to increased upwelling around Antarctica and an increase in silica supply to Subantarctic Mode Water formation. The resulting pulse of silica-rich waters was rapidly transferred north to the Equatorial Undercurrent and thence via the subsurface Mexican Coastal Current to the Gulf of California. Overall, the sequence shows a resurgence in El Niño strength and an intensification of the North American Monsoon associated with Northern Hemisphere warming on the transition to Greenland Interstadial 12. Penetration of tropical waters to the Gulf was aided by El Niño events. Diatom production in the summer stratified waters was in the subsurface, tapping nutrients from the nutricline. Marine varves up to 9 mm thick record as many as 8 within-year flux events. Repeated summer flux events of actively reproducing diatoms in subsurface blooms were driven by recurrent intense monsoonal Gulf surge storms. Around 60% of *A. nodulifera* cells examined were actively dividing and every stage of the cell division cycle is represented. Other diatom species record renewed vigour of winter – spring upwelling associated with strengthening northwesterly winds as the North Pacific high migrated northward. The monsoon intensification, the resurgence in El Niño strength and the strengthened winter-spring northwesterlies were likely all driven by the reduction to a minimum extent of the Laurentide Ice Sheet in Greenland Interstadial 12. The changes recorded in this transition to a warm interstadial may serve as an indicator of future changes in the region driven by global warming.

## 1. Introduction

Laminated diatomaceous pelagic and hemipelagic sediments often constitute palaeo-sediment traps that record successive flux events allowing reconstructions of ancient seasonal and interannual variability (Kemp, 2003; Schimmelmann et al., 2016). The diatom blooms recorded within individual laminae are episodic, typically seasonal events, and the spring bloom, for example, commonly forms pulses of export flux resulting from post-bloom aggregation and rapid sinking of diatom cells and colonies (Alldredge and Goltschalk, 1989; Billett et al., 1983). Diatom laminae may also be generated by flux from deep chlorophyll maximum concentrations, commonly forming within the thermocline that may grow and accumulate over periods of weeks or months in the summer (Kemp and Villareal, 2018). Such deep concentrations are commonly disrupted when water column mixing by autumn/winter storms breaks down stratification leading to the "fall dump" flux (Kemp et al., 2000; Sancetta et al., 1991). In oceanic settings giant diatoms or diatom mats may be concentrated and generate massive, potentially lamina-forming flux by interaction with oceanic convergences along major frontal systems (Kemp et al., 2006) or in the fronts around

* Corresponding author.
*E-mail address:* aesk@soton.ac.uk (A.E.S. Kemp).

https://doi.org/10.1016/j.quascirev.2024.108929
Received 3 June 2024; Received in revised form 13 August 2024; Accepted 25 August 2024
Available online 4 September 2024

mesoscale eddies or rings (Rackebrandt et al., 2011). Although millimeter- to centimeter-scale laminae may be subsampled using conventional techniques, the full resolution available in laminated diatomaceous sediments is best exploited using scanning electron microscope (SEM) methods (Brodie and Kemp, 1994; Grimm et al., 1997). This enables the reconstruction of sub-seasonal processes and up to 19 separate sub-laminae per year have been identified (Dean et al., 2001). The availability of sufficiently continuous laminated intervals facilitates the development of time-series long enough to capture variation in interannual modes of climate variability, for example, the El Niño-Southern Oscillation (ENSO) (Bull et al., 2000; Chang et al., 2003; Davies et al., 2012; Dean et al., 2001; Pike and Kemp, 1997).

The Gulf of California (hereafter the 'Gulf', Fig. 1) became a classic location for laminated marine sediments with the pioneering work of Calvert who identified annual sediment couplets (varves) comprising of a clay-rich and a diatom-rich component (Calvert, 1966). This annual sedimentation model was verified and developed by work on Kasten cores (Donegan and Schrader, 1982), on box cores (Baumgartner et al., 1985) as well as from the first DSDP piston coring of Site 480 on Leg 64 (Shipboard-Scientific-Party, 1982; Schrader et al., 1980; Schrader, 1982). Comparison of varved sediments spanning the recent to the early Holocene with sediment trap data from the central Gulf demonstrates preservation of the seasonal cycle of diatom production and flux in the sediment record (Baumgartner et al., 1985; Pike and Kemp, 1996a; Sancetta, 1995; Thunell et al., 1993; Thunell, 1998). These studies revealed an intriguing mixture of typical coastal bloom diatom taxa including *Chaetoceros* spp. with those of more oceanic affinity reflecting the penetration of eastern tropical Pacific waters into the Gulf.

The common diatoms of the coastal ocean are well studied; many of the species are in culture and much of the understanding of diatom ecology has been based on such research. By contrast, the diatoms characteristic of the open ocean are far less encountered, and their sampling is often serendipitous, a question of "being in the right place, at the right time". In such circumstances, the ecological information available from the "palaeo-sediment traps" of laminated sediments may be used to inform modern oceanographic studies. While the oceanic diatom *Azpeitia nodulfera* has rarely been identified as a major component of Holocene laminated sediments in the Gulf, it was a more significant contributor in pre-Holocene, late Pleistocene intervals (Barron et al., 2014) although it has hitherto not been documented as a "bloom" species.

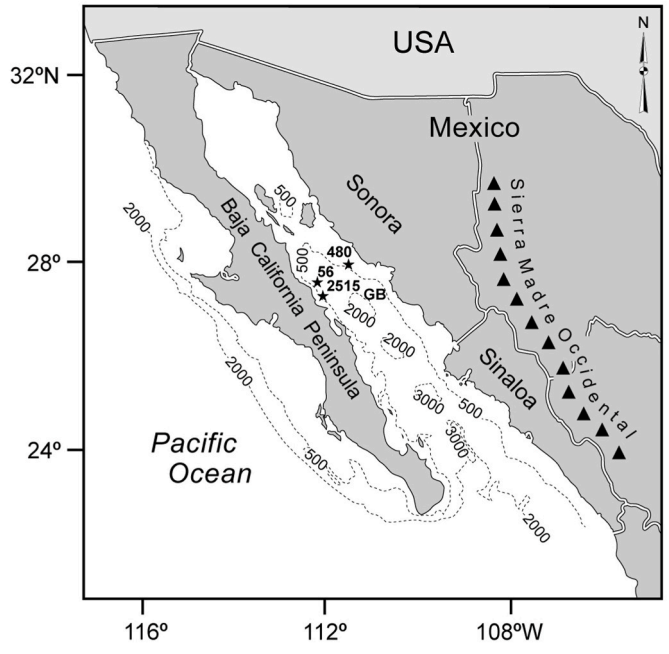


**Fig. 1.** Gulf of California and the location of core MD02-2515 and other cores mentioned in the text. GB – Guaymas Basin.

New scanning electron microscope (SEM) analysis of Late Pleistocene laminated sediments from the central Gulf has revealed abundant and thick (1.27 mm on average) near-monospecific laminae of the tropical diatom *Azpeitia nodulifera*, which has not previously been identified as a lamina-forming constituent in any setting. The aims of this paper are to document an interval rich in near-monospecific *A. nodulifera* laminae and to investigate the palaeoecological and palaeoceanographic implications of these flux events. Lamina production and deposition mechanisms are discussed, including the occurrence of abundant dividing cells within the *A. nodulifera* laminae that indicate active vegetative reproduction was ongoing before abrupt sinking and sedimentation took place. The sub-annual resolution afforded by the laminated sediments allows the *A. nodulifera* laminae to be placed in the context of the seasonal cycle of diatom production and sediment deposition and the climatic drivers. Lastly, we consider the broader palaeoclimatic and palaeoceanographic implications of the *A. nodulifera* laminae, and the relation to changes in oceanic and atmospheric circulation related to northern hemisphere climate variability including the Dansgaard/Oeschger (DO) Cycles.

## 2. Regional setting and previous work

We first review the modern climate and oceanography of the Gulf (Fig. 1) on a seasonal to interannual basis to provide a context for the interpretation of our record. To complement this, we then describe the current understanding of the seasonal cycle of sediment flux in the Gulf from a synergy of water column observations and sediment analysis followed by a brief account of the prior understanding of the ecology of *Azpeitia nodulifera*. Regarding recent palaeoceanographic studies, work on the Holocene has been reviewed by Douglas et al. (2007). Extensive geochemical and micropaleontological research on the 55 kyr record of core MD02-2515, the subject of this study, has been reviewed by Barron et al. (2014) and we refer to relevant aspects of this in the Douglas et al. (2007)Discussion section including the papers of Pichevin et al. (2012) and Chang et al. (2015).

### 2.1. Climate and oceanography

#### 2.1.1. The monsoonal climate of the Gulf

Seasonal variability is tightly coupled to the monsoonal climate of the Gulf within the North American Monsoon (NAM) system. Strong northwesterly winds that drive upwelling along the mainland coast through winter and spring (November to May, but most intense in January to April), are replaced as the East Pacific High and the ITCZ shift northwards in the summer monsoon by weaker southerly winds that are strongest in July and August (Badan-Dangon et al., 1991; Bordoni et al., 2004; Bray and Robles, 1991). The winter to early spring upwelling generates productivity and high pigment concentrations are observed across the Gulf with phytoplankton blooms also fueled by the redistribution of nutrients by transient mesoscale features such as eddies and jets (Badan-Dangon et al., 1991; Badan-Dangon et al., 1985; Garcia--Morales et al., 2017; Santamaría-del-Angel et al., 1994). Decline of the northwesterly winds allows the Mexican Coastal Current to gradually penetrate northward bringing an influx of tropical Pacific surface waters so that by mid-summer there is a thick (up to 150 m) warm surface layer in the southern and central Gulf and the resultant strong and deep thermocline restricts nutrient supply and limits production in surface waters (Badan-Dangon et al., 1991; Bray and Robles, 1991; Godinez et al., 2010). The propagation of the 26 °C SST isotherm into the Gulf appears to represent a threshold for triggering the monsoon and the bulk of the monsoonal rainfall that is concentrated on the western slopes of the Sierra Madre Occidental occurs when SST in the northern Gulf exceeds 29 °C facilitating stronger convection (Mitchell et al., 2002). The

NAM precipitation delivers up to 70% of the total annual rainfall of northwestern Mexico (Pascale and Bordoni, 2016). Precipitation is enhanced by a strong diurnal "sea-breeze" effect that draws in moisture over the mountains (Douglas and Li, 1996). The episodic occurrence of the most vigorous convective thunderstorms of the monsoon are related to northward surges of cooler, moister tropical air known as "Gulf surges" whose initiation and intensity are linked to the passage of mid-tropospheric tropical easterly wave troughs (Fuller and Stensrud, 2000; Pascale and Bordoni, 2016) or of tropical cyclones (Higgins and Shi, 2005). Wind speeds within Gulf Surges may exceed 20 m/s (Force 9) (Rogers and Johnson, 2007) and they generate convection that brings severe thunderstorms that typically develop in the late afternoon (Adams and Comrie, 1997). The most intense of these may generate Chubasco winds that can approach hurricane strength (Idso, 1976). The frequency of Gulf Surges is typically three to four per month (Bordoni and Stevens, 2006; Fuller and Stensrud, 2000), with an average of 15 in the 21 June – 30 September Monsoon season (Pascale et al., 2018). The numbers of stronger surges vary from 4 to 18 per year and the annual summertime rainfall increases with increasing numbers of Gulf Surges (Pascale and Bordoni, 2016).

#### 2.1.2. El Niño and La Niña influences on the Gulf

The principal source of interannual variability within the Gulf arises from the El Niño/Southern Oscillation (ENSO) (Baumgartner and Christensen, 1985; Bray and Robles, 1991; Lavin et al., 2003). Anomalous sea conditions associated with El Niño events in the Gulf include enhanced flow of tropical waters into the Gulf accompanied by an increase in sea surface temperatures (SSTs) and a deepening of the winter pycnocline (Robles and Marinone, 1987; Soto-Mardones et al., 1999). During the 1982–1983 El Niño, while upwelling continued, the deepened thermocline resulted in lower nutrient enrichment (Lluch-Cota, 2000). Analysis of satellite-derived SST anomalies between 1984 and 2000 revealed positive anomalies of up to 3 °C associated with El Niño and negative anomalies of up to 4 °C associated with La Niña (Lavin et al., 2003). The SST increases are most pronounced in winter indicating a combination of disruption of wind-driven upwelling via atmospheric teleconnections and a deepening of the thermocline (Herrera-Cervantes et al., 2007). The El Niño anomalies may be explained by coastally-trapped Kelvin waves which propagate poleward along the eastern tropical Pacific coast and drive the increased penetration of tropical surface waters to the Gulf (Baumgartner and Christensen, 1985; Lavin et al., 2003; Strub and James, 2002). More broadly, this strong Kelvin wave activity generated by El Niño results in episodic intensification of the poleward Mexican Coastal Current that delivers tropical waters to the sub-tropical eastern Pacific and to the Gulf, thus deepening the thermocline (Gomez-Valdivia et al., 2015) (Fig. 2). This linkage is also important for delivery of potentially nutrient-rich, sub--thermocline waters to the Gulf, since the Mexican Coastal Current starts in the sub-surface, tapping waters from the Equatorial Undercurrent via the North Tsuchiya Jet (Kessler, 2006) (Fig. 2).

The surface water productivity in the modern Gulf in the region of the Guaymas Basin has been monitored, between 2002 and 2015, by satellite determinations of chlorophyll *a* (Chl-a), integrated with SST and wind intensity data (Garcia-Morales et al., 2017). El Niño periods are characterized by elevated SST, reduced northwesterly wind speeds and decreased Chl-a, whereas La Niña episodes feature reduced SST, enhanced northwesterly wind speeds and elevated Chl-a. This builds on earlier research including Herrera-Cervantes et al. (2007); Kahru et al. (2004); Lluch-Cota (2000), and demonstrates that the peak winter to early spring, upwelling-driven production in the Gulf occurs during La Niña, with the lowest during El Niño.

#### 2.1.3. El Niño influences on the North American monsoon in the Gulf region

The consensus of earlier analyses was for a weakening of the North American Monsoon during El Niño with an overall reduction of precipitation in western Mexico but with a corresponding monsoonal strengthening and increased rainfall with La Niña (Higgins and Shi, 2001; Vera et al., 2006). However, recent, more detailed analysis of long-term regional precipitation records show a more complex pattern. In fact, in the borderlands of the Gulf (northern Sinaloa, Sonora and the Baja Peninsula, Fig. 1), summer precipitation is maintained or enhanced during El Niño and reduced during La Niña (Bhattacharya and Chiang, 2014; Morales et al., 2023; Seager et al., 2009). Whereas El Niño summers are associated with decreased precipitation in SW Mexico (Higgins et al., 1999), strong convection and high rainfall is maintained over NW Mexico including the Gulf coast/Sierra Madre Occidental by mechanisms that may include tropical storms as well as the main monsoon (Reyes and Mejía-Trejo, 1991; Seager et al., 2009). Wet summer conditions may also be maintained during the transition from El Niño to La Niña (Zolotokrylin et al., 2016). Thus, during El Niño, a vigorous monsoon is present in the Gulf in summer, with its associated Gulf surges that deliver much of the precipitation. Conversely, during La Niña summers, convective activity in the Gulf is suppressed and rainfall reduced (Morales et al., 2023; Seager et al., 2009), see summary in Table 1.

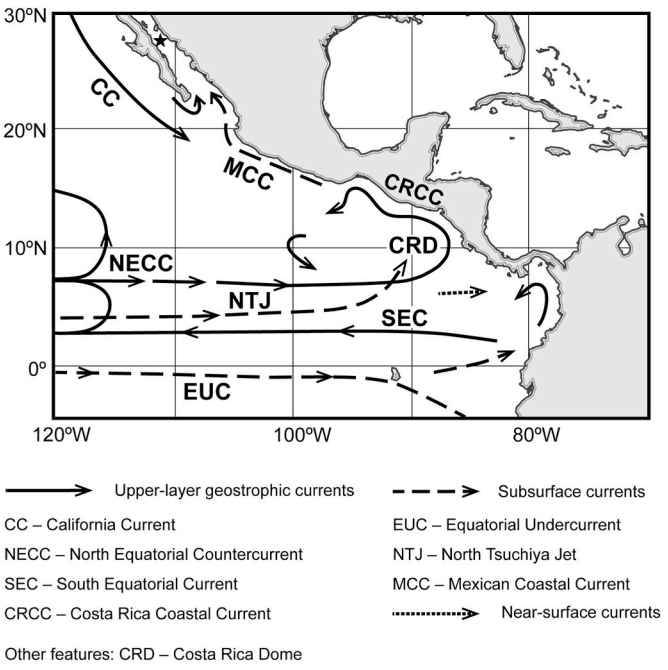


**Fig. 2.** Schematic circulation in the eastern tropical Pacific showing surface and subsurface (sub-thermocline) currents adapted from Kessler (2006) and Gomez-Valdivia (2015).

On longer decadal – multidecadal timescales, variability has been related to the Pacific Decadal Oscillation (PDO) and the North Pacific Oscillation/North Pacific Gyre Oscillation (NPO/NPGO) (Castro et al., 2001), while links to the Atlantic Multidecadal Oscillation (AMO) highlight teleconnections driven by variation in North Atlantic SST (Morales et al., 2023; Sutton and Hodson, 2005). While AMO positive regimes (e.g. 1931–1960) adversely affect rainfall in the central and southwestern US and eastern Mexico there is a relatively minor effect in western Mexico and the monsoon penetrates to the central Gulf in both regimes (Hu and Feng, 2008). Variations on longer millennial and stadial/interstadial timescales are dealt with in the discussion section.

### 2.2. The seasonal cycle of production and flux in the modern/Holocene Gulf

#### 2.2.1. Insights into the seasonal cycle from sediment traps

A six year sediment trap study in the Guaymas Basin shows a broad variation with biogenic opal flux (mainly diatoms) dominant from fall to

**Table 1**
Summary of the effect of El Niño and La Niña on Gulf ocean and atmosphere behaviour, based on the references given in 2.1.2 and 2.1.3.

| Season | ENSO neutral | El Niño | La Niña |
|---|---|---|---|
| Winter – early Spring | • Northwesterly winds drive upwelling<br>• (strongest January to April) | • Thermocline deepened<br>• Upwelling winds suppressed | • Upwelling winds strengthened |
| Summer Monsoon season (June–September) | • Weak southerly winds<br>• Tropical ocean waters penetrate Gulf; increase water column stratification<br>• Monsoon "Gulf Surge" storms move to NW up the Gulf | • Increased influx of tropical ocean waters<br>• Thermocline deepened | • Reduced SST – decreased stratification<br>• Atmospheric convection and monsoon activity reduced |

spring and lithogenic flux prevalent in the summer (Thunell, 1998). In more detail, the opal flux often contains two major pulses with one from October–December (fall – early winter) and another from February–April (late winter – spring) (see Fig. 6 of Thunell, 1998). Analysis of diatoms in the traps reveals a spring flux of typical upwelling/spring bloom, small genera such as *Chaetoceros* (hyalochaete) (present as both vegetative stages and resting spores) and *Thalassionema* and *Skeletonema* (Sancetta, 1995). By contrast, the fall – early winter flux is dominated by a maxima in cell volume contributed by large taxa including rhizosolenids and *Coscindiscus* spp., with a mixed assemblage occurring throughout the winter (Sancetta, 1995). (Note that we use the term rhizosolenids to encompass those taxa within the family *Rhizosoleniaceae,* including, in the Gulf, mainly the genera *Rhizosolenia* and *Dactyliosolen* and the species *Proboscia alata*, *Pseudosolenia calcar-avis* and *Guinardia flaccida*.)

The late winter – spring diatom flux tallies with the upwelling-driven surface production observed by satellite. However, there is generally less of a satellite/surface chorophyll signal over the Guaymas Basin corresponding to the fall-early winter diatom flux (Garcia-Morales et al., 2017), even though the fall flux may be equivalent to or greater than that of the winter-spring. This is because the large diatoms typical of the "fall dump" flux are adapted to growing in stratified conditions at depths below the reach of satellite sensors (Kemp et al., 2000) – see discussion in 2.2.2, below.

The summer lithogenic flux is driven by the monsoonal storms, with delivery by aeolian transport of particles by convective thunderstorms and/or by subsequent river runoff (Baumgartner et al., 1991; Thunell, 1998). The occurrence of benthic and coastal diatoms amongst the lithogenic material suggests storm-generated suspension and off-shelf transport (Sancetta, 1995).

The sediment trap study of Thunell (1998) included measurement of the opal, carbonate, organic carbon and lithogenic mass fluxes. Biogenic opal comprised typically 75% of the mass flux and was deemed a better indicator of biological production and flux than organic carbon. A decoupling between weight % organic carbon and biogenic opal also occurs throughout the MD02-2515 record, and this has been ascribed variously to greater uptake by diatoms of Si under Fe-limitation during intense blooms and/or a dilution effect (Pichevin et al., 2012; Chang et al., 2015).

### *2.2.2. Insights into the seasonal cycle from recent/holocene laminated sediments*

The first studies of lamina composition were based on subsampling of individual laminae directly from sediment cores (Baumgartner et al., 1985; Donegan and Schrader, 1982). The resolution of these analyses was insufficient to identify changes of diatom composition within individual laminae, however changes in the bulk diatom composition of individual laminae were used to make inferences on interannual variability (see 2.2.3, below).

The seasonal sequence of diatom flux has also been documented using backscattered electron imagery (BSEI) of resin-embedded sediment to study Holocene varved sediments from the central Gulf from cores JPC56 and JPC48 (Fig. 3). Diatom laminae immediately below the summer lithogenic laminae are dominated by *Chaetoceros* (hyalchaete) with rarer *Skeletonema*, both taxa being typical of the spring bloom/

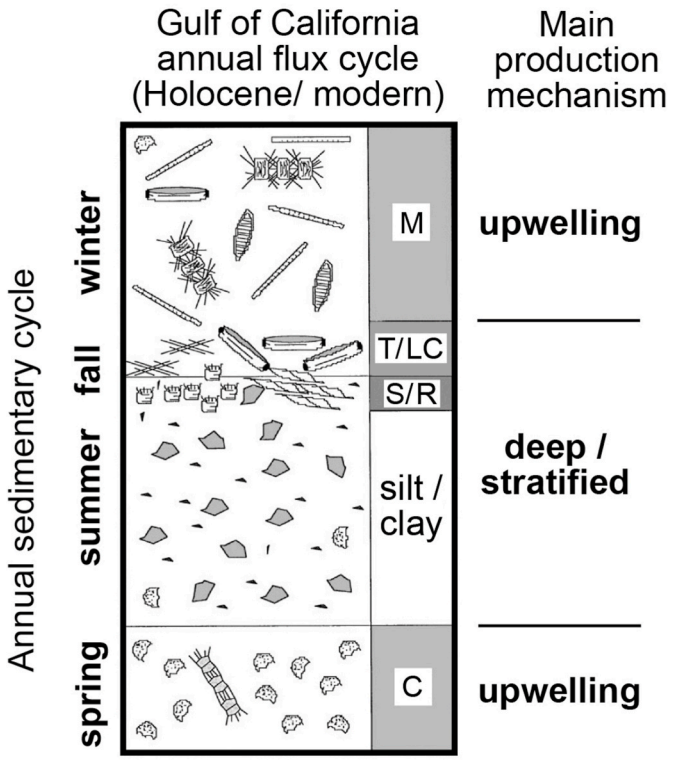


**Fig. 3.** Summary of the modern/Holocene annual Gulf flux cycle observed from laminated sediments (Pike and Kemp, 1996a; Kemp et al., 2001) and water column studies (Sancetta, 1995; Thunell et al., 1993). C- *Chaetoceros*, S – *Stephanopyxis*, R – *Rhizosolenia*, T – *Thalassiothrix*, LC – large *Coscinodiscus*, M – mixed diatom assemblage.

upwelling pulse. Contrasting, near-monospecific laminae (that is, diatom ooze laminae which are predominantly composed of a single species or genus) of large *Coscinodiscus* spp., *Rhizosolenia* spp., *Stephanopyxis palmeriana* and *Thalassiothrix longissima* are found just above the summer lithogenic laminae of clay and silt, indicating a fall/early winter period of deposition (Pike and Kemp, 1996a, 1997) (Fig. 3). These laminae are thought to result from production at depth by adaptation to growth in low light in a deep chlorophyll maximum (DCM) or through buoyancy regulation (some rhizosolenids) during summer stratified conditions. Subsequent deposition occurs when the thermocline breaks down in autumn/early winter in the "fall dump" (Kemp et al., 2000; Pike and Kemp, 1997; Sancetta, 1995; Sancetta et al., 1991). Evidence from the comparison of the $\delta^{15}N$ signatures of diatom-bound organic matter between diatom size fractions (<63 μm/> 63 μm) in Holocene Gulf sediments provides corroborative evidence that the larger diatoms, mainly *T. longissima* and large *Coscinodiscus* spp. in this instance, grew under stratified conditions at the base of the euphotic zone, under low light levels and in excess nitrate (Kalansky et al., 2011). From a satellite chlorophyll *a* sensor, the Gulf might be expected to show one major seasonal burst of production in the winter/spring. However, the specially adapted species of the "shade flora" are able to thrive in the

summer stratified conditions and generate as much or more flux in the fall dump, at breakdown of stratification, than the winter/spring blooms (Kemp et al., 2000; Kemp and Villareal, 2018; Pike and Kemp, 1997; Sancetta, 1995).

#### 2.2.3. Interannual variability from sediment traps and recent/Holocene laminated sediments

There is conflicting evidence from the limited data. Based on elevated opal fluxes in the 1995–96 "non-El Niño" year in the 1990–1996 sediment trap series, Thunell (1998) proposed an overall decline in production during El Niño. However, there was no distinction in the contribution of upwelling versus fall dump diatom taxa to this total since the diatom study of the traps (Sancetta, 1995) only extended from 1990 to 1992. On the other hand, in a dated 20 year varve record (1953–1972) from the Guaymas slope, El Niño years coincided with the highest density of individuals (total number of diatoms and silicoflagellates per $cm^2$) and the dominance of a warm water assemblage including high abundances of *Azpeitia nodulifer* (Baumgartner et al., 1985). Interestingly, the main interannual variability in sediment trap taxa occurs with El Niño, with *A. nodulifera*, otherwise very rare in traps, reaching up to 5%, and taken to represent the presence of warm eastern tropical Pacific waters penetrating further into the Gulf during El Niño conditions (Sancetta, 1995). A factor analysis of minor taxa combining sediment trap and Core (JPC 56) data gave a factor dominated by *A. nodulifera*, and again, this was interpreted to represent increased penetration of subtropical water into the Gulf (Sancetta, 1995).

Laminae rich in *A. nodulifera* were briefly noted based on the macroscopic subsampling of laminae from DSDP Site 480 in the eastern Guaymas Basin (Donegan and Schrader, 1982; Schrader, 1982; Schrader et al., 1980). Based on the warm water affinity of *A. nodulifera* and the absence of the silicoflagellate upwelling indicator *Octatis pulchra*, these laminae rich in *A. nodulifera* were interpreted to represent an "oceanic end member" relating to the summer influx of oceanic waters to the Gulf (Donegan and Schrader, 1982; Schrader, 1982).

Time series analysis of the occurrence of *Thalassiothrix longissima* diatom mats in Holocene laminated sediments revealed significant periodicities of mat deposition at ~11, 22–24, and ~50 years and these were originally ascribed to solar cycle influence (Pike and Kemp, 1997). Such periodicities are now known to be characteristic of the Pacific Decadal Oscillation (PDO) (Skakala and Bruun, 2018), which is related to longer term changes in the amplitude of El Niño variability, although a 22-year periodicity in PDO has itself been linked to solar influence (McCabe-Glynn et al., 2013).

### 2.3. Prior understanding of the ecology of Azpeitia nodulifera

*Azpeitia nodulifera* (basionym *Coscinodiscus nodulifer*) is generally described as a heavily silicified, planktonic diatom characteristic of warm tropical waters which has not been reported to occur in colonies (Fryxell et al., 1986) and first appeared in the tropical Pacific around 13.3 Ma (Barron, 2003). More broadly, *A. nodulifera* has been found in plankton tow and sediment trap samples from the equatorial Pacific, where it is never in high concentrations and has been regarded, generally, as a minor component of oceanic warm water assemblages (Iriarte and Fryxell, 1995; Kobayashi and Takahashi, 2002; Takahashi et al., 2009). Rare occurrences in relatively high abundance in surface sediments or cores have been ascribed to resistance to dissolution (Lange and Berger, 1993; Schrader and Sorknes, 1991; Seeberg-Elverfeldt et al., 2004a; Warnock et al., 2007). The only prior indication of possible sedimentation of water column concentrations are the existence of thick layers of *A. nodulifera* co-occurring with *Coscinodiscus* spp.in laminated sediments from the Red Sea (Seeberg-Elverfeldt et al., 2004b). In offshore – onshore surface sediment-sampling transects, it is generally very rare or absent in shelf or coastal stations (Pokras and Molfino, 1986; Schuette and Schrader, 1981). In other occurrences in eastern equatorial Pacific cores, it has been regarded as a tropical oceanic, warm water indicator (Devries and Schrader, 1981; Romero et al., 2011).

From previous sediment trap and sediment laminae studies mentioned in 2.2.3 above, *Azpeitia nodulifera* is regarded as an indicator of the influx of tropical oceanic waters into the Gulf and has been associated with El Niño. Palaeoceanographic studies in the Gulf have also generally associated increases in the relative abundance of *A. nodulifera* in the sediment record as an indicator of the incursion of tropical waters into the Gulf with a particular association with sustained El Niño activity (Barron and Bukry, 2007; Barron et al., 2004, 2005). In their synthesis of the MD02-2515, 55 kyr record, Barron et al. (2014) characterize its ecology as representing "Tropical Pacific, deeply stratified waters".

## 3. Materials, methods and dating

The piston core MD 02–2515 (27°29.01 N, 112°04.46 W, 64.4 m long, 881 m water depth) was retrieved by the *Marion Dufresne* in 2002 from the Guaymas Basin (Beaufort and Scientific Party, 2002, Fig. 1). Sediments consist of mm-scale laminated diatomaceous muds with intermittent intervening homogenous intervals. The samples analysed here were taken from core sections 45, 4–139 cm and 46, 0–78 cm, corresponding to a void corrected core depth of 5136–5343 cm, following the depth scale used in Pichevin et al. (2012). MD 02–2515 is well dated with an age model based on linear interpolation of 26 AMS $^{14}C$ dates measured on bulk organic matter and 2 AMS $^{14}C$ dates measured on foraminifera (Pichevin et al., 2012). We therefore adopt this age model which was also used in the subsequent papers of Chang et al. (2015), Cheshire and Thurow (2013), McClymont et al. (2012), Barron et al. (2014). Beyond 40 ka the age model is less robust and the calendar age of 46,418 ka from 5238 cm, near the top of the interval studied has a 1 sigma error of 2184 years. For correlation to global events, we use the updated chronology of the NGRIP GICC05 (Svensson et al., 2008) as adopted by the INTIMATE event stratigraphy of Rasmussen et al. (2014),which gives an age of 46,860 b2k for the start of GI-12. A varve-based age "floating" chronology for the studied interval is presented in the results section. The duration of the studied interval is shown in Fig. 4a in relation to the GICC05 NGRIP oxygen isotope record and to the wt. % opal and $\delta^{15}N$ records of Pichevin et al. (2012) and Chang et al. (2015) and the depth interval is shown with the detailed opal record in Fig. 4b.

Slab samples were taken from split cores using the cookie cutter method (Dean et al., 1999; Kemp et al., 2001). Slabs were first x-rayed and then sub-samples were embedded with Spurr low-viscosity epoxy resin to make polished thin sections (PTS) for backscattered electron imagery (BSEI) analysis using the methods of Pike and Kemp (1996b) and Kemp et al. (1998). Samples were examined at high magnifications using the SEM and were logged lamina-by-lamina using an ×73 magnification BSEI photomosaic as a basemap noting the occurrence of lithogenic and biogenic components. Varve identification was based on grey scale, X-radiograph and BSEI, in combination (Fig. 5). Laminae, within the varve, were defined based on changes in sediment composition that were distinctive and laterally continuous and from these, the seasonal flux sequence was reconstructed. Sequential, distinct, near-monospecific *A. nodulifera* laminae are differentiated by abrupt and laterally traceable changes in *A. nodulifera* abundance and/or matrix content. Thickness measurements of laminae were obtained from BSEI using the method of Francus et al. (2002), taking the average of three thickness measurements per lamina. Stub samples were prepared from sediment counterparts of the embedded material, split parallel to the laminae, then dried and gold coated to produce topographic images for diatom species identification.

Previous studies have proposed that variations in the diameter of *A. nodulifera* may be climatically controlled with populations with cell diameters greater than 60 μm characteristic of high nutrient concentrations (Bromble and Burckle, 1983; Burckle and McLaughlin, 1977; Burckle et al., 1981; Lange and Berger, 1993). This motivated an

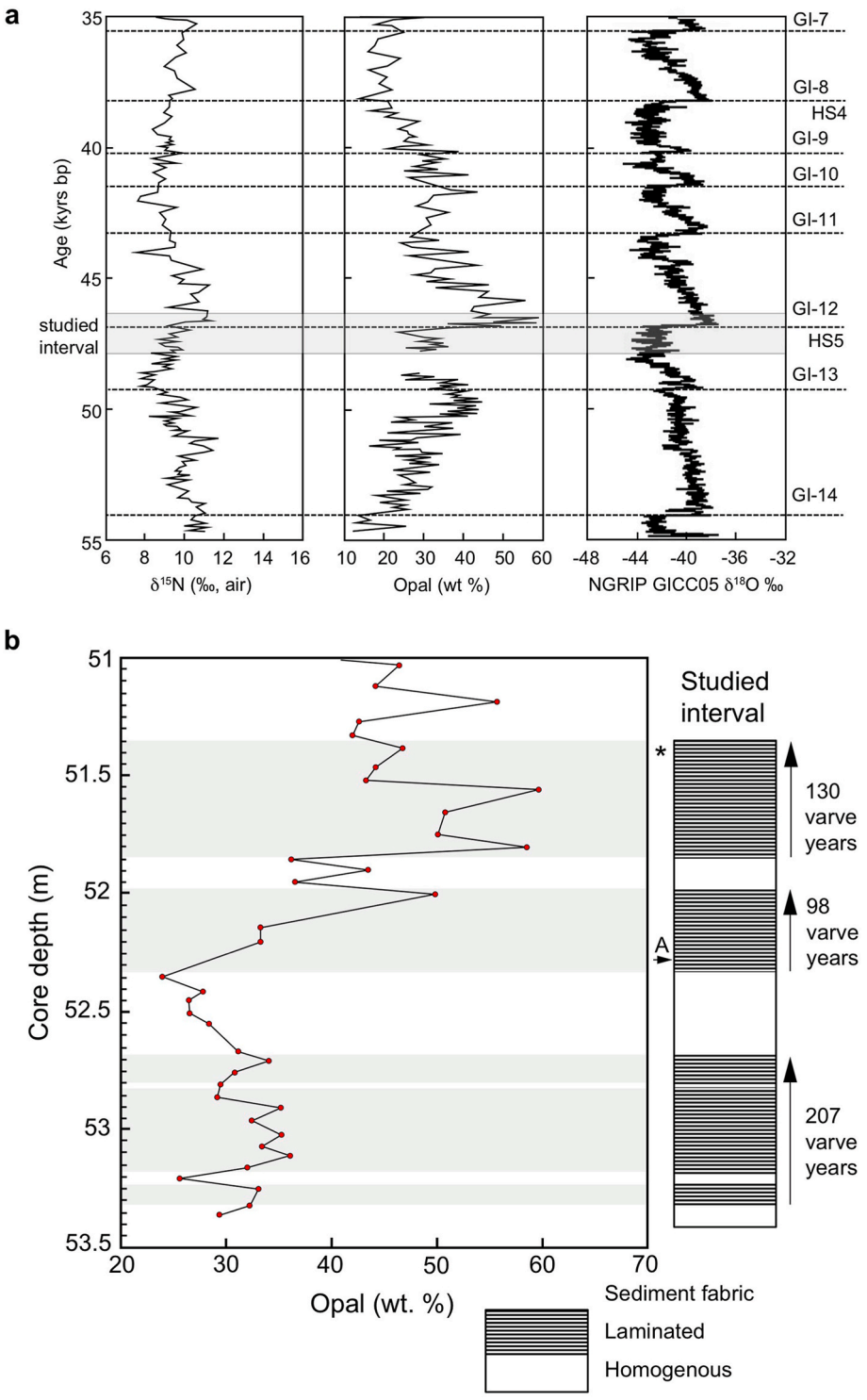


**Fig. 4.** a) Duration of the studied interval in relation to the GICC05 NGRIP oxygen isotope record and to the weight % biogenic silica and $\delta^{15}N$ records of Pichevin et al. (2012) and Chang et al. (2015). b) Detail of the studied interval showing extent of laminated segments and weight % biogenic silica (Pichevin et al., 2012) plotted against depth in core. The star marks the depth of the radiocarbon date of 46,418 Calendar age. The arrow "A" indicates the point in the middle laminated segment where *Azpeitia nodulifera* replaces *Coscinodiscus* spp. as the dominant fall dump diatom in the lamina sequence.

investigation into size variations of *A. nodulifera* within the near mono-specific laminae. Strew slides were made of three *A. nodulifera* laminae taken from the top, middle and base of the top laminated segment (5145, 5155, 5173 cm core depth respectively). Samples were taken using toothpicks, and then disaggregated and suspended in deionized water. The suspension was pipetted onto a glass cover slip that was left to dry slowly on a hot plate before being mounted onto a glass slide using Norland Optical Adhesive #61 (refractive index = 1.56). For each slide, the diameters of 300 *A. nodulifera* frustules were measured using a calibrated reticule at ×400 magnification under optical

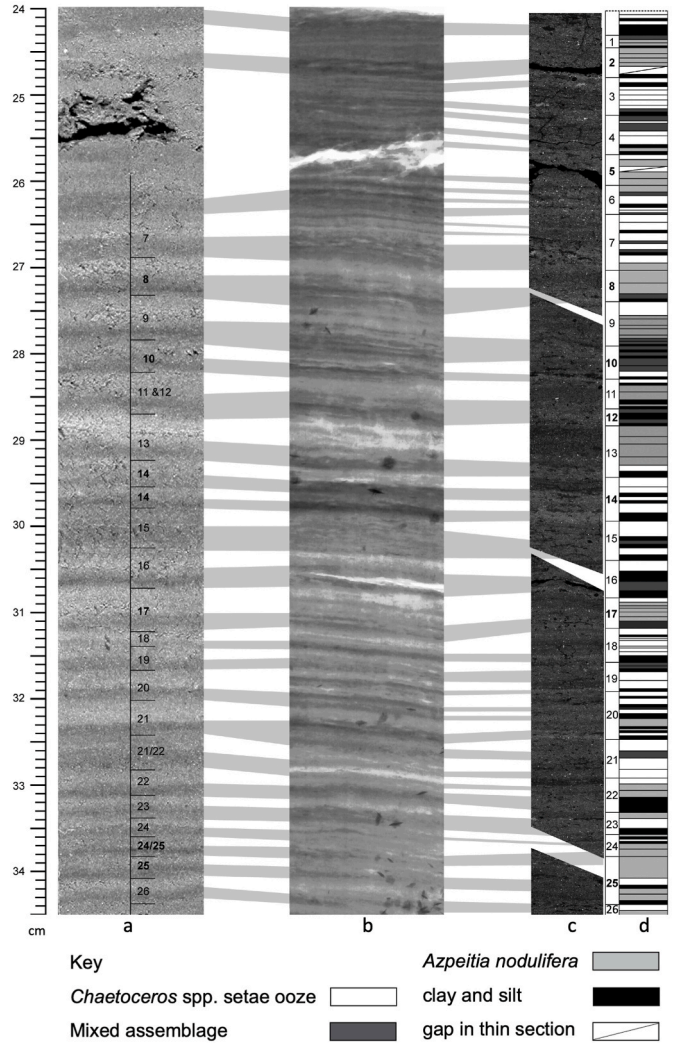


**Fig. 5.** Example showing comparison of different imaging methods and detailed logs based on BSEI from core interval Section 45, 24–35 cm (Core Depth 5156–5167 cm). a) - shows grey-scale image of split core surface showing alternation between pale and dark laminae comprising an apparent annual couplet of alternating terrigenous and diatomaceous sediment. b) - shows x-ray of the 1 cm-thick slab, in which more complexity and intra-annual variability is evident. c) – low magnification mosaic of each successive polished thin section. d) – Detailed log based on high magnification BSEI imagery of low mag base maps.

microscopy.

Time series were compiled, and spectral analysis was undertaken on the total diatom ooze thickness per varve, on the total lithogenic thickness per varve and the number of *A. nodulifera* laminae per varve. Prior to spectral analysis, any outliers, defined here as any value greater than the mean plus 2.5 × the standard deviation, were removed and replaced with this limit. The Fourier transform treats the data as though it is infinitely repeated, therefore any trend present in the dataset will produce a spectral peak with the same frequency as the length of the time-series and to avoid this, each dataset was detrended using a linear function. The time-series were examined for step changes as this will also result in distortion of the spectra. Hiatuses can affect the detection of high frequency cycles and alter the frequency of any cycles identified (Weedon, 2003), however no hiatuses were identified during the careful inspection of the sedimentary record during BSEI analysis. Spectral analysis was undertaken using the REDFIT method using REDFIT version 3.5 (Schulz and Mudelsee, 2002).

## 4. Results

### 4.1. Annual lamina sequences and varve identification

The sediment investigated comprises a 207 cm – long interval containing three near consecutive laminated segments containing regular alternations between clay and silt-rich lithogenic laminae with diatomaceous laminae with two intervening segments of bioturbated/homogenous diatomaceous mud (Fig. 4b). The lower, middle, and top laminated segments comprise of 207, 98 and 130 varves respectively with two very thin bioturbated/homogenous interruptions to the lower segment (Fig. 4b). The duration of the entire interval is estimated at 655 years, based on taking an average varve thickness through the homogenous sections. This is likely to be an underestimate since the diatom and opal concentration is relatively lower in the homogenous segments, reflecting a lower sedimentation rate. Furthermore, in keeping with previous studies of JPC 56 (Sancetta, 1995), there is evidence of diatom dissolution in the bioturbated/homogenous sediment. Identification of repeated sequences allows the typical varve structures to be described.

### 4.2. Sedimentation and biogenic opal accumulation rates

Average sedimentation rates for the whole interval may be calculated using the age model-derived duration of 1417 years (146 cm/ka) or the varve-derived age model of 655 years (316 cm/ka). The peak sedimentation rate estimated based on the top laminated segment which had the largest average varve thickness is 380 cm/ka. The average opal accumulation rate for the whole interval may be calculated using the average dry bulk density value for the core of 0.26 g/cm$^3$ (Chang et al., 2015; Beaufort and Scientific Party, 2002) and the average biogenic opal of the interval of 36.3 % (Chang et al., 2015) to give 13.8 g/cm$^2$/kyr. Based on the varve-derived age model the rate is 29.8 g/cm$^2$/kyr, while the peak rate in the top laminated segment is 59 g/cm$^2$/kyr (using the average opal content for this segment).

We do not have direct dry bulk density measurements for the studied interval, and it may be argued that the average for the core is likely to be too great, since the most diatom-rich sediment in the top laminated segment would have a lower density due to the open framework of the frustules. Taking a value of 23 g/cm$^3$ derived from the most diatom-rich laminated intervals of DSDP Site 480 from the Guaymas Basin (Shipboard-Scientific-Party, 1982) would give a biogenic opal accumulation rate of 52 g/cm$^2$/kyr or 520 g/m$^2$/yr for the peak rate in the top laminated segment (full Interstadial).

### 4.3. Variation in varve characteristics in the three varved segments

The average varve thickness ranges from 3 mm in the lower segment to 3.7 and 3.8 mm, respectively in the middle and top segments and are more than twice the thickness of the typical Holocene varves. The top segment has the highest opal concentration (Fig. 4b), containing the purest diatom ooze and has some of the thickest varves ranging exceptionally up to 9 mm. The lower and middle segments, most commonly have just two laminae per varve whereas the top segment has an average of five laminae in each varve, marked mainly by additional discrete *A. nodulifera* laminae (Fig. 6). The lithogenic laminae are typically 1–1.5 mm thick and comprise very fine to coarse silt, minor clay and minor very fine sand grade material. There is a distinction in the diatom composition, particularly regarding the near-monospecific laminae (Table 2). The diatom laminae in the lower segment are comprised of near monospecific *Coscinodiscus* spp., near monospecific *A. nodulifera* or a mixed diatom assemblage, with *A. nodulifera* becoming more dominant towards the top. In the middle segment, only the lowermost 16 varves contain *Coscinodiscus* spp. laminae and thereafter they comprise either near monospecific *A. nodulifera* or a mixed diatom assemblage (Fig. 6). The main contributors to the mixed assemblage laminae include *Thalassionema nitzschiodes*, *Hemidicus cuneiformis*, *Actinoptychus* spp.,

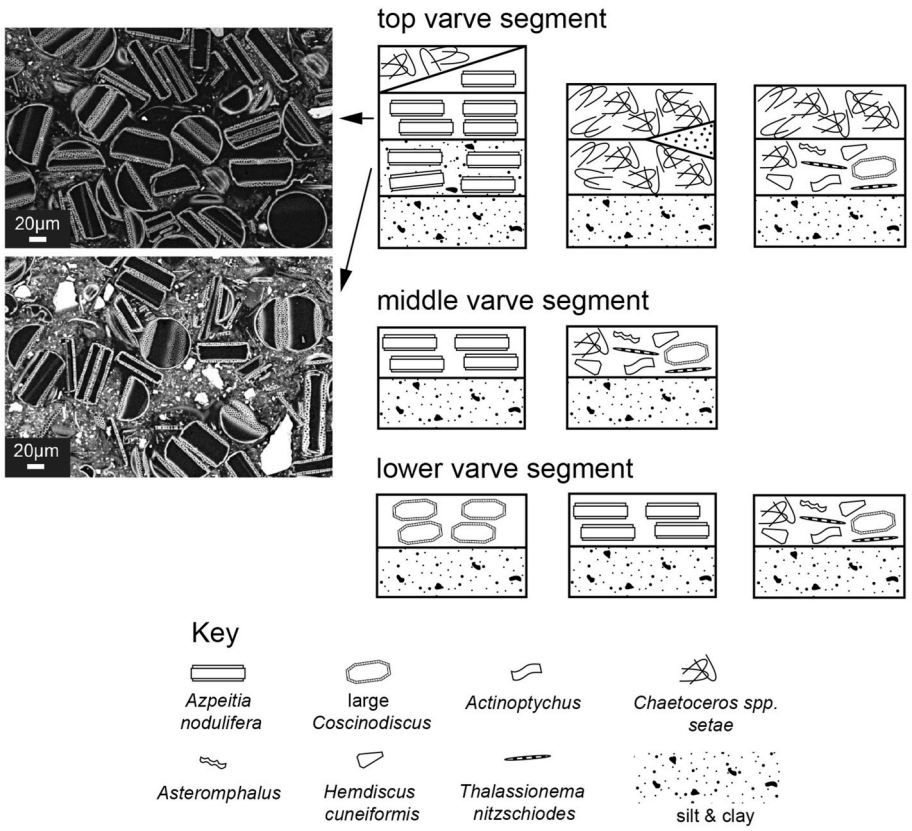


**Fig. 6.** The typical laminae present in varves in the lower, middle and top laminated segments. BSEI images show the different types of near-monospecific *A. nodulifera* laminae. For the top segment, the upper image shows nearly pure *A. nodulifera* concentrations; the lower image shows *A. nodulifera* in a typical matrix of clay and silt.

**Table 2**
Number of the three most common near-monospecific laminae per varve segment.

| Segment | *A. nodulifera* laminae | *Chaetoceros setae* ooze laminae | Large *Coscinodiscus* laminae |
|---|---|---|---|
| Top (130 varve years) | 132 | 142 | 4 |
| Middle (98 varve years) | 51 | 3 | 9 |
| Lower (207 varve years) | 59 | 12 | 40 |

*Asteromphalus* spp. and large *Coscinodiscus* spp. (Fig. 7). The top segment, by contrast, contains no *Coscinodiscus* spp. laminae, and displays an alternation between varves dominated by *Chaetoceros setae* (55) (Fig. 7a and b) and *Azpeitia nodulifera* (52) (Figs. 5, 6 and 8). In the *Azpeitia nodulifera* – dominated varves, there is commonly a thin or discontinuous *Chaetoceros setae* lamina cap. The *Chaetoceros setae* laminae do not contain *Chaetoceros* resting spores and only rarely include the very lightly silicified vegetative cells to which the *setae* attach (Fig. 7b). They may include a very thin or discontinuous lithogenic lamina.

### 4.4. *Azpeitia nodulifera laminae*

Near-monospecific laminae of *A. nodulifera* are present throughout the interval investigated with an average lamina thickness of 1.27 mm (standard deviation (s.d.) = 0.8 mm) for the whole interval (see Table 2 for individual segments). The lower and middle varved segments of 207 and 98 varve years include 52 and 46 varves (respectively) dominated by near-monospecific *A. nodulifera* laminae. These varves consist of a couplet of a clay/silt lamina and a near-monospecific *A. nodulifera* lamina (Fig. 6). In the top varved segment of 130 varve years, there are 52 varves which are dominated by near-monospecific *A. nodulifera* laminae, these varves generally consist of laminae comprising of clay/silt followed by one or more, (up to 7) near-monospecific *A. nodulifera* laminae that may be overlain by a thin or discontinuous *Chaetoceros setae* ooze top (Fig. 6).

Sequential, intra-annual laminae were identified by a clear and abrupt change in matrix composition and/or *A. nodulifera* abundance, and these were classified as separate depositional (flux) events (Fig. 6). Such multiple laminae were mainly confined to the top varve segment. The matrix surrounding the *A. nodulifera* frustules may consist predominantly of clay and silt, or of centric diatom fragments with a more minor clay and silt component. Where sequential *A. nodulifera* laminae were encountered, the lower laminae generally contained silt and clay while the topmost generally had minimal lithogenic content (Fig. 6). The near-monospecific *A. nodulifera* laminae, contain minor amounts of *Actinoptychus* sp., *Coscinodiscus* spp., and occasional *Asteromphalus* sp., *Fragilariopsis doliolus, Hemidiscus cuneiformis* and *S. palmeriana.* There are three laminae in the middle segment that are co-dominated by both *A. nodulifera* and *S. palmeriana*, and ten laminae in the lower segment that are co-dominated by both *A. nodulifera* and large *Coscinodiscus*.

### 4.5. *Preservation and size range of A. nodulifera*

Warnock et al. (2007) devised a preservation index in which individual cells of *A. nodulifera* may be placed into one of four categories

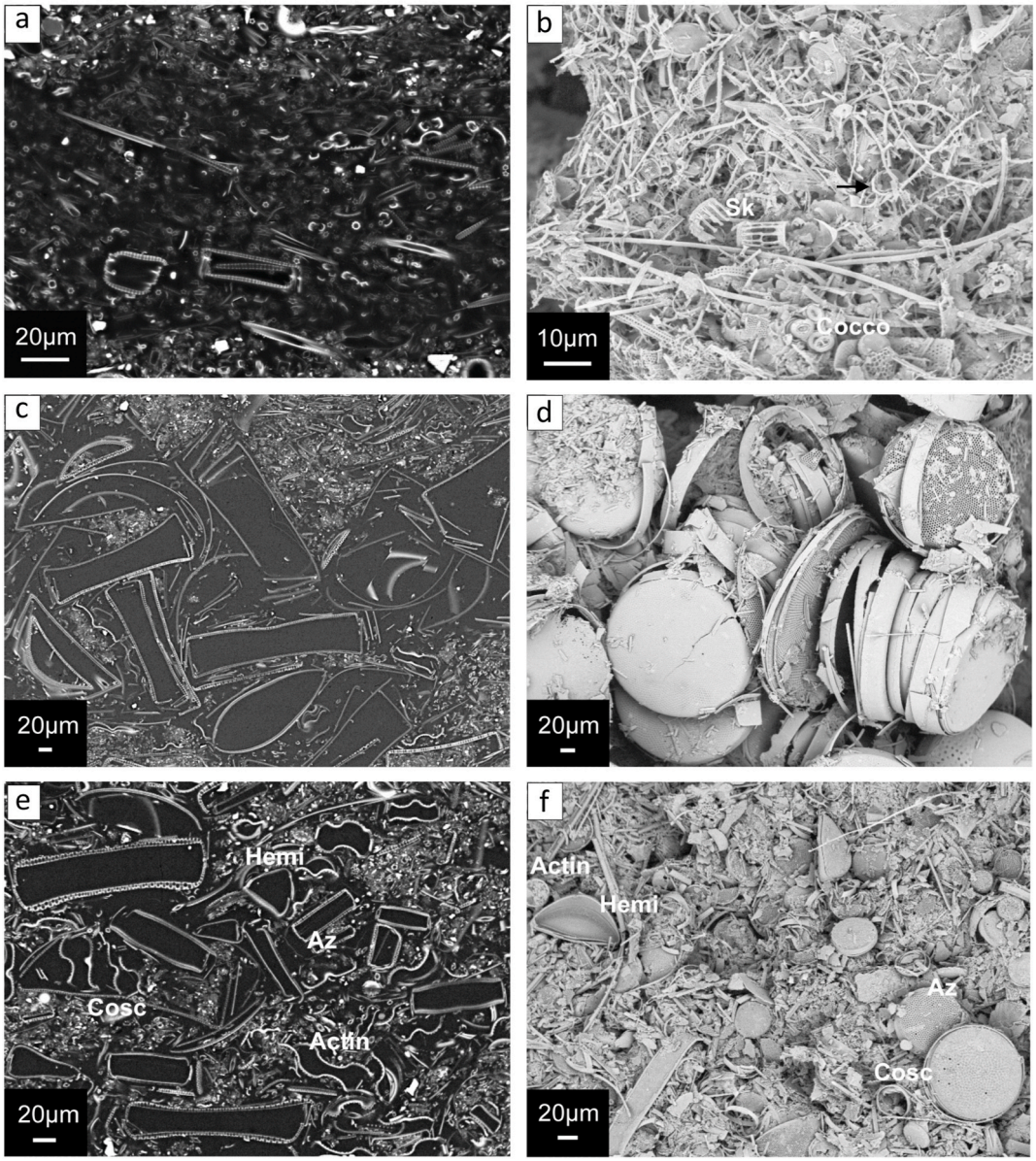


**Fig. 7.** Common components of laminae in BSEI of polished thin sections (left panels) and topographic stub images (right panels). a) and b): concentrations of *Chaetoceros* spp *setae*, mainly visible as cross sections in BSEI; in b) note the characteristic bifurcation of some *setae* and a rarely preserved vegetative cell (black arrow); c) and d): large *Coscinodiscus* sp., e) and f): mixed assemblage. Abbreviations: Cocco – coccoliths, Sk – *Skeletonema*, Hemi – *Hemidiscus*, Actin – *Actinoptychus*, Cosc – *Coscinodiscus*, Az – *Azpeitia.*

based on the state of the velum, a uniform perforate silica microstructure that covers the areolae known as a cribrum (pl. cribra). Cells with a fully intact vela/cribra are placed into state one (indicating the least dissolution), cells where the vela and all pegs around the areolae are completely dissolved are placed into state four (indicating high dissolution levels) (Warnock et al., 2007). Topographic images indicate that the *A. nodulifera* cells documented here generally have an intact velum indicating that they fit into 'state one' and are in the highest state of preservation (Fig. 8e and f).

To investigate variations in cell diameters, 300 *A. nodulifera* cells were counted using optical microscopy from three samples selected from near-monospecific *A. nodulifera* laminae at core depths of 5145, 5155, 5173 cm, giving mean cell diameters of 70 μm (s.d. 8), 66 μm (s.d. 9) and 71 μm (s.d. 6), respectively.

### 4.6. Linking of cells and evidence for vegetative division

Topographic BSEI shows that *A. nodulifera* commonly occurs in stacks of ~2–7 frustules particularly in the top laminated segment (Fig. 8a–d). Stacks occur at various orientations suggesting they do not simply form as a result of cells settling but rather that the cells may have been linked together in the water column. Adjacent, stacked pairs of frustules tend to be similar but not identical in size (e.g., Fig. 8d), suggesting that cells may be the product of vegetative division with the inner valves of the pairs therefore represent sibling valves.

BSEI of the polished thin sections allows the cross sections of the valves to be examined and reveals abundant dividing cells (diatom cells which are undergoing mitotic division) (Fig. 9). Dividing cells are observed throughout the interval and a complete range of stages in division are seen ranging from immediately prior with a maximal number of girdle bands, through the progressive formation of the new valves to final separation. The excellent preservation facilitates a detailed

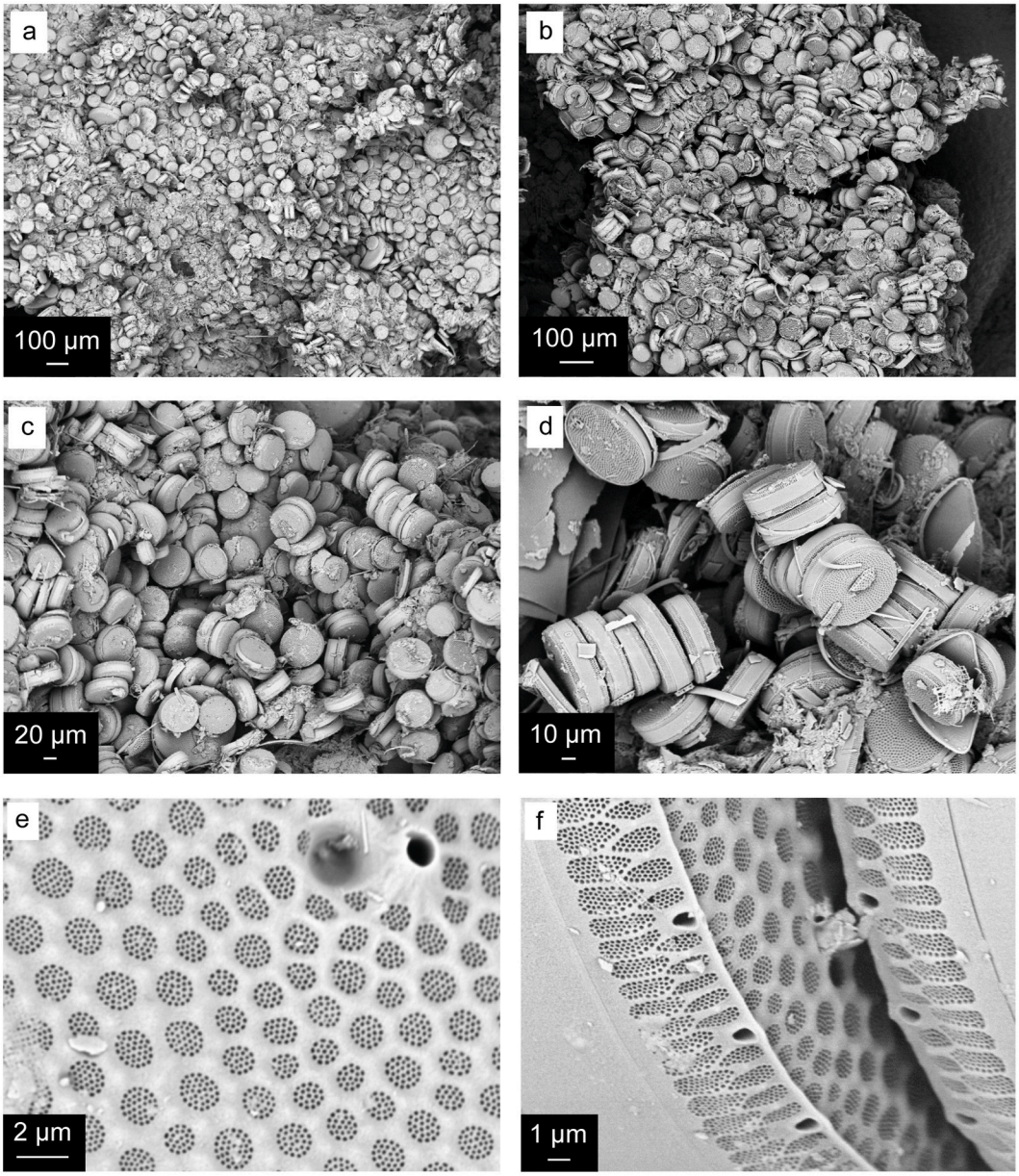


**Fig. 8.** Topographic SEM images of *A. nodulifera* in stub samples, note 'stacks' of frustules. a) A near monospecific concentration of *A. nodulifera* with silt and clay sized lithogenic material. The occasional larger centric diatoms are *Coscinodiscus* sp. b) Monospecific concentration of *A. nodulifera* with some stacks of frustules evident. c) and d); Detail showing monospecific concentrations of *A. nodulifera* with stacks of differing numbers of cells. e) The excellent preservation state demonstrated by valve areolae with fully intact vela (pores) or cribra (perforate layers of opal); also (top right in e) note the characteristic central depression and raised external opening of the central rimoportula. f) Valve exterior showing the two rows of elongate mantle aureolae with complete and intact pores and the marginal rimoportulae (three visible on each valve).

illustration of the diatom girdle through this process (Fig. 9g). Examination of valve cross sections in BSEI show up to ~60% of cells are in various stages of division with the highest proportions in the top laminated segment.

### 4.7. Time series analysis

Results of the time series and spectral analysis of variation in the total diatom ooze thickness per varve, the total lithogenic thickness per varve and the number of *A. nodulifera* laminae per varve are given in Fig. 10. Emphasis was placed on periodicities exceeding the 95% confidence interval.

## 5. Discussion

The overall varve composition superficially resembles that of the Holocene/recent varves (Fig. 3). The main differences are the presence of the near-monospecific *Azpeitia nodulifera* laminae which do not occur in the Holocene/recent varves and the presence of multiple discrete diatom laminae within one year. We first discuss the ecological significance of the *A. nodulifera* laminae and then consider the broader palaeoceanographic and palaeoclimatic implications.

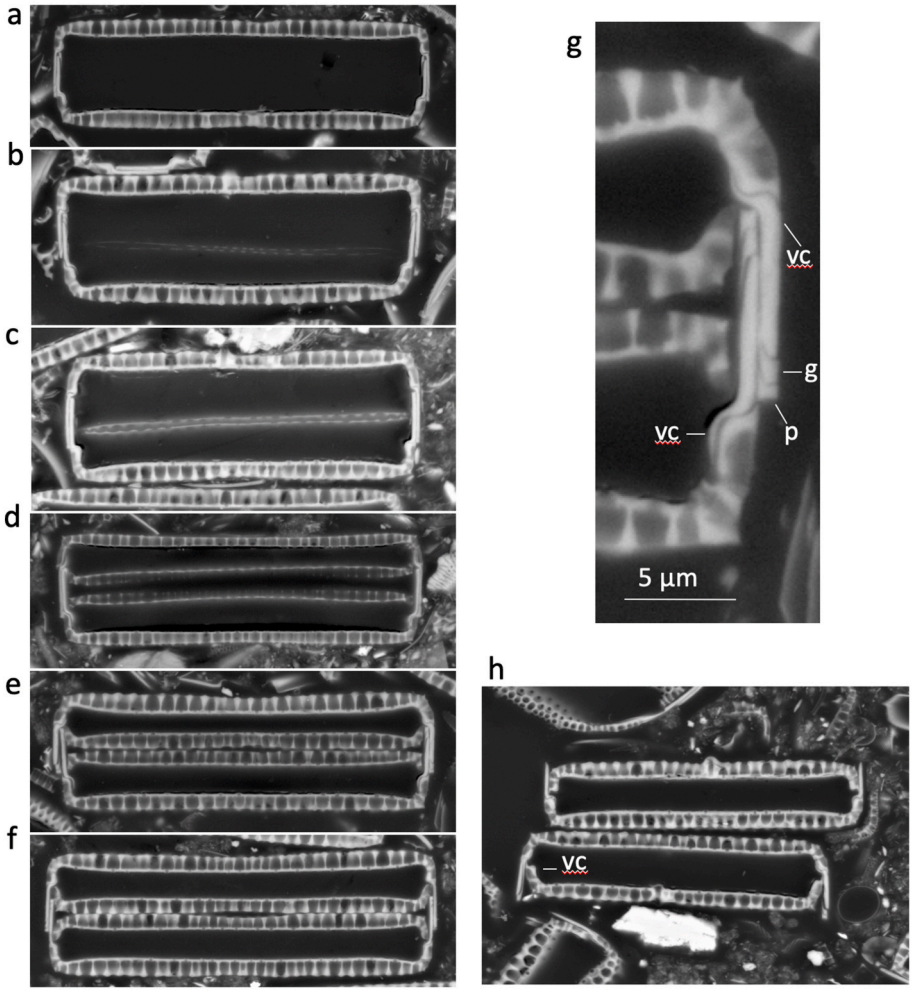


**Fig. 9.** Cells of *A. nodulifera*, showing different stages of the cell division cycle (diameter of frustule = length in image given for each panel), a) Prior to division (80 µm), b) first sign of valve deposition (73 µm), c) the two new valves (hypothecae) become distinct (68 µm), d) the two new valves have separated (70 µm), e) immediately prior to division, the two new sibling valves are fully formed and linked to the parent valves (74 µm). f) onset of division, the girdle bands are moving apart and separation of the cells has begun (85 µm). g) Detail of right-hand side of (e) to illustrate the structure of the girdle, vc – valvocopula (the girdle band proximal to the valve), g – girdle band, p – pleural band (the most distal girdle band). In the right-hand panel, separation of the cells has begun. h) Detail showing two newly divided cells (although unlikely to be siblings given the orientation) with prominent epicingula and note the newly forming valvocopula (vc arrowed) in the newly formed hypovalve of the lower cell (diameter of topmost valve = length in image = 66 µm).

### *5.1. Origins of the near-monospecific laminae of Azpeitia nodulifera and the seasonal cycle of the Gulf*

#### *5.1.1. The A. nodulifera laminae represent flux from bloom events*

There has been a tendency to suggest that concentrations of robust oceanic diatoms (whose ecology is often poorly understood) may originate from the dissolution of more lightly silicified species. There is also some indication that this may occur elsewhere with *A. nodulifera*, for example in the Red Sea, where a relative abundance in the water column of 0.6–1.5% contrasts with sediment abundances of 34.5–41.5 % (Seeberg-Elverfeldt et al., 2004a). However, with the abundant evidence of outstanding preservation from the present samples (Fig. 8), we may dismiss this "preservation" explanation and instead seek to identify scenarios that would have produced high water column concentrations of *A. nodulifera* with subsequent rapid delivery to the sediment. The size range of our specimens, all >60 µm, places them within the size grouping characteristic of high nutrient supply (Burckle and McLaughlin, 1977; Murray and Schrader, 1982). Taken together with the abundant evidence for vegetative cell division (Figs. 6 and 9), extensive and repeated diatom blooms offer the best explanation.

#### *5.1.2. Ecology of the A. nodulifera blooms*

Any mechanism proposed for the blooms of *A. nodulifera* needs to take into account its affinity with warm-water, stratified conditions and the co-occurrence in some laminae with either *S. palmeriana* or large *Coscinodiscus* spp., suggesting a shared mode of production. Both of these associated taxa are typical of the fall dump whereby large diatoms that have the ability to grow at depth in stratified conditions during the summer are deposited when autumn or winter storms generate mixing and destroy stratification (Kemp et al., 2000).

The typical fall dump taxa are large or colonial oceanic diatoms, and they are enabled to bloom in stratified conditions by one or more adaptations that facilitate growth in the lower part of the euphotic zone. The most likely adaptation in the case of *A. nodulifera* is the ability to grow at depth under low light conditions in a deep chlorophyll maximum, and this has been demonstrated experimentally in the case of *S. palmeriana* (Goldman, 1993; Goldman and McGillicuddy, 2003). The large size of these diatoms is also an adaptation to a pulsed nutrient supply since their large vacuole enables luxury uptake and storage of nutrients (Stolte and Riegman, 1996). The monospecific concentrations of *A. nodulifera* that are especially common in the top laminated segment likely record maximum penetration of tropical waters, carrying seed

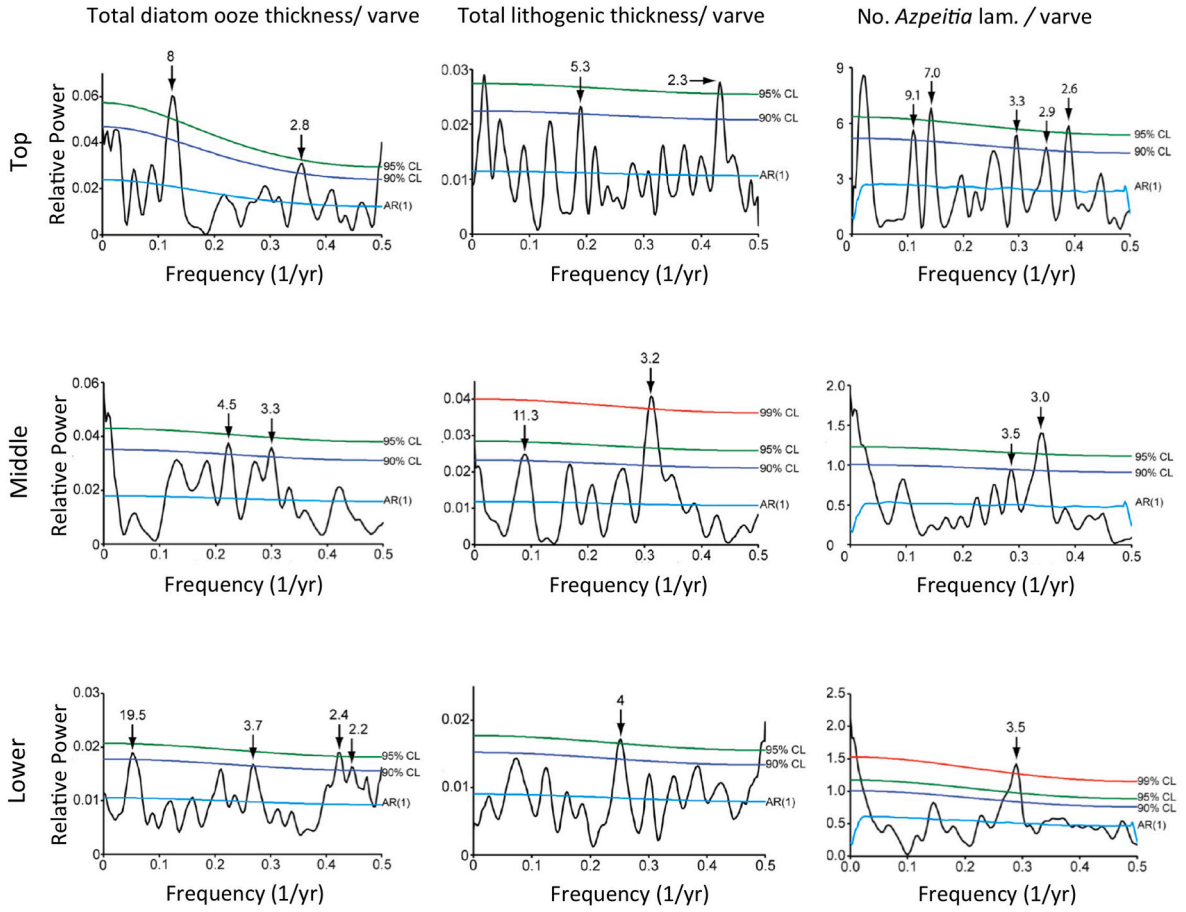


**Fig. 10.** Spectral analysis of variation in diatom ooze thickness per varve, lithogenic sediment thickness per varve and number of *A. nodulifera* laminae per varve.

populations into the Gulf.

### 5.1.3. Evidence for cell division suggests flux during blooms not at the end or post bloom

A remarkable feature of the *A. nodulifera* laminae, particularly in the top varve segment is that more than half of the cells appear to be at some stage in the process of cell division (clearly seen in the BSEI of the resin embedded sections cut perpendicular to laminae, Figs. 6 and 9). Although in most cases there appears to be a very slight reduction in the diameter of the daughter cells, in others there appears to be negligible reduction (Fig. 9). This minimal reduction appears to be, in part, enabled by the high curvature of the valvocopula (Fig. 9). In fact, this has been observed in other diatom species (Rose and Cox, 2013), and the generalization of the "size-reduction" paradigm for vegetative cell division may be an over-simplification for all diatoms. We have not observed any auxospores in the material so there is no direct record of a sexual phase that has been hypothesized to generate massive flux, for example, for the Antarctic diatom *Corethron* (Crawford, 1995). Ourselves and colleagues have worked on a total of more than 50,000 years of records in varved laminated diatomaceous sequences ranging in age from modern to Cretaceous and we have hitherto observed little or no evidence for vegetative cell division "in progress". The classical scenario for the post "spring bloom" flux is where exhaustion of nutrients triggers rapid post-bloom flocculation and mass sedimentation (Alldredge and Gotschalk, 1989); the so-called "self-sedimentation" of Grimm et al. (1997). This type of "post-bloom" flux either generates sedimentation of non-dividing cells or of resting spores or resting stages in those taxa adapted to produce them. Likewise, in observations of taxa whose flux has been generated by interactions with frontal zones or by disruption in the fall dump (including the Holocene Gulf varves) we have only rarely observed cell division in process. By contrast, in the case of the *A. nodulifera* laminae, cells were actively and vigorously reproducing at the time of flux, and, in the case of the top laminated segment, around 60% of cells were undergoing vegetative reproduction. Evidently, the mass flux was generated by some external forcing that occurred during the height of the blooms.

### 5.1.4. Position of Azpeitia nodulifera laminae in the annual flux and productivity cycle and significance of multiple intra-annual flux events

There is a significant contrast between the fall dump flux as documented in the modern/Holocene sediments of the Gulf (Fig. 3) (Pike and Kemp, 1996a, 1997; Kemp et al., 2000) and that observed here. The Holocene fall dump laminae generally document the sequential flux of different species groups with those likely most vulnerable to water column agitation (rhizosolenids) first in the sequence followed by large centrics including *Coscinodiscus* and these sublaminae are rarely repeated within an individual year. Furthermore, silt and clay generally only co-occur with the rhizosolenids. In contrast there are multiple (up to 7) sequential *A. nodulifera* laminae corresponding to multiple distinct flux events present in the top laminated segment - the closest to the full stadial. The lower of these multiple lamina sets commonly also contain silt and clay suggesting that they were co-sedimented with the detrital input from monsoon storm activity (Fig. 6). Importantly, the active cell division in the *A. nodulifera* laminae indicate that the blooms were still vigorously active and not near termination (e.g. through lack of nutrients). We therefore interpret these successive intra-seasonal laminae to record repeated flux events from actively blooming diatom populations triggered by storm-driven disruption of stratification. After the storm-induced turbulence had abated and stratification had been re-established, sufficient seed populations had evidently persisted in the

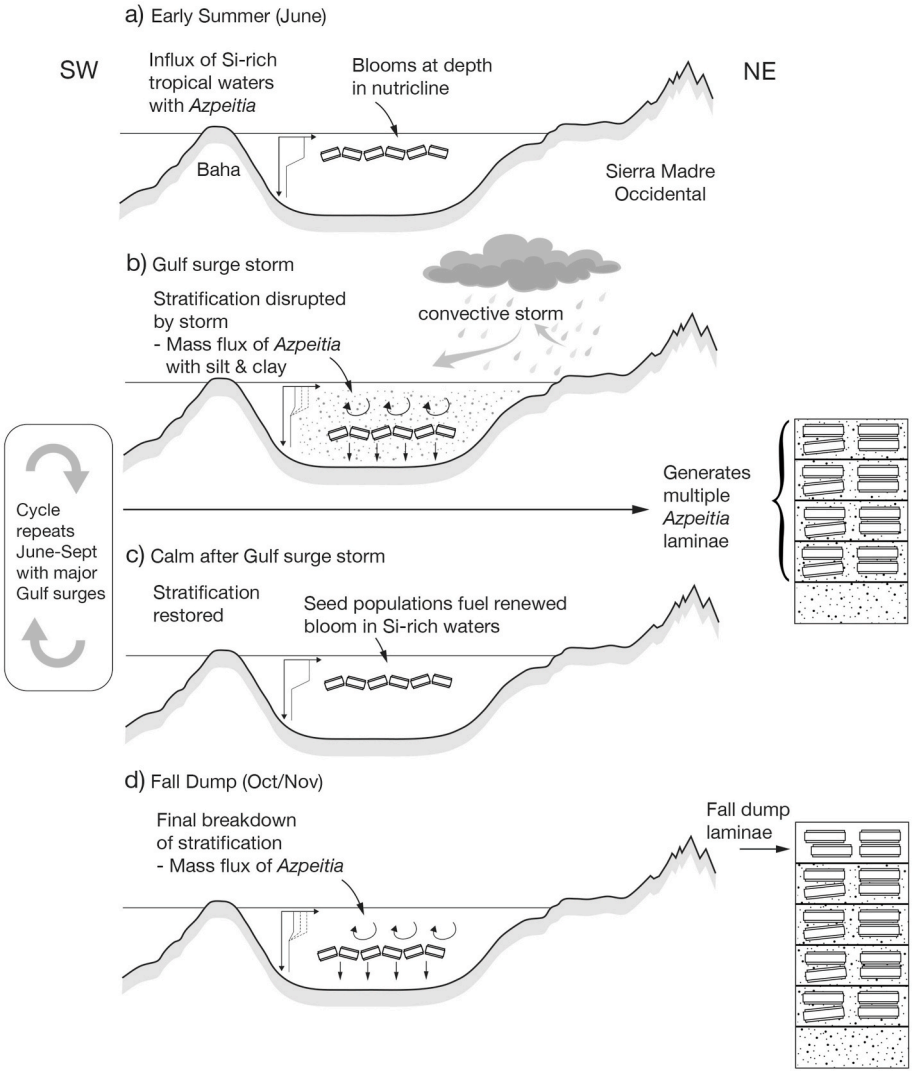


**Fig. 11.** Generation of multiple *A. nodulifera* flux events during the summer monsoon period by recurrent Gulf surge storms.

water column to recommence the blooms. Thus, the multiple flux events were likely driven by multiple successive monsoonal storms in any given year, indicating a dynamic monsoon system (Fig. 11). The topmost *A. nodulifera* laminae in the varves are purer with minimal lithogenic material, more resembling the typical, October–November fall dump laminae of the Holocene (Figs. 6 and 11).

A further contrast is that in the early Holocene record, the fall dump lamina is generally followed by a winter mixed flora upwelling lamina and then a spring upwelling lamina, representing a seasonal cycle close to the modern Gulf (Kemp et al., 2000; Pike and Kemp, 1997; Sancetta, 1995). Similar mixed assemblage laminae are generally absent from *A. nodulifera*-dominated varves. This suggests that the presence of *A. nodulifera* marked periods where prolonged stratification continued into winter, related to a deeper and/or stronger thermocline, thus inhibiting the more typical winter/spring production.

### 5.1.5. *Increasing dominance of A. nodulifera marks increasing penetration of tropical waters into the Gulf*

In the lower varve segment near-monospecific laminae of large *Coscinodiscus* spp. are more common than *A. nodulifera* laminae. In fact, large *Coscinodiscus* spp are a common component of the typical modern and Holocene flux cycle in the Gulf (Fig. 3). Near-monospecific laminae of large *Coscinodiscus* spp. are also common in the earliest 16 varve years of the middle varve segment but are very rare thereafter and *A. nodulifera* laminae become the dominant large diatom in the laminae (Fig. 4b). This suggests that there was progressively increased penetration of tropical waters into the Gulf with local taxa being displaced and outgrown by incoming seed populations of oceanic diatoms. This was evidently concomitant with increasing supply of silica to the Gulf.

### 5.1.6. *Laminae of Chaetoceros setae mark increased upwelling driven by strengthened winter-spring northwesterly winds*

The rarity of *Chaetoceros setae* laminae (evidencing flux from the spring bloom) in the lower and middle segment suggests suppression of upwelling, a deeper or stronger thermocline and/or the presence of less Si-rich waters. The presence of common *Chaetoceros setae* laminae in the top laminated segment suggests increases in upwelling strength, a decrease in stratification intensity and/or an increase in nutrient supply. Given evidence for abundant silica availability throughout the studied interval (see 5.2.1, below), an increase in upwelling intensity appears more likely. In fact, this would be consistent with the interstadial warming. Palaeoceanographic evidence from diatoms and silicoflagellates demonstrates rapid increases in upwelling indicators in the transition to the Bolling Allerod (GI-1) and in the earliest Holocene (Barron et al., 2004). This increased upwelling was likely driven by initiation of strong winter northwesterly winds along the Gulf in response to northward migration of the North Pacific High to its current position (Lora et al., 2016) (Fig. 12). Prior to these deglacial/interstadial

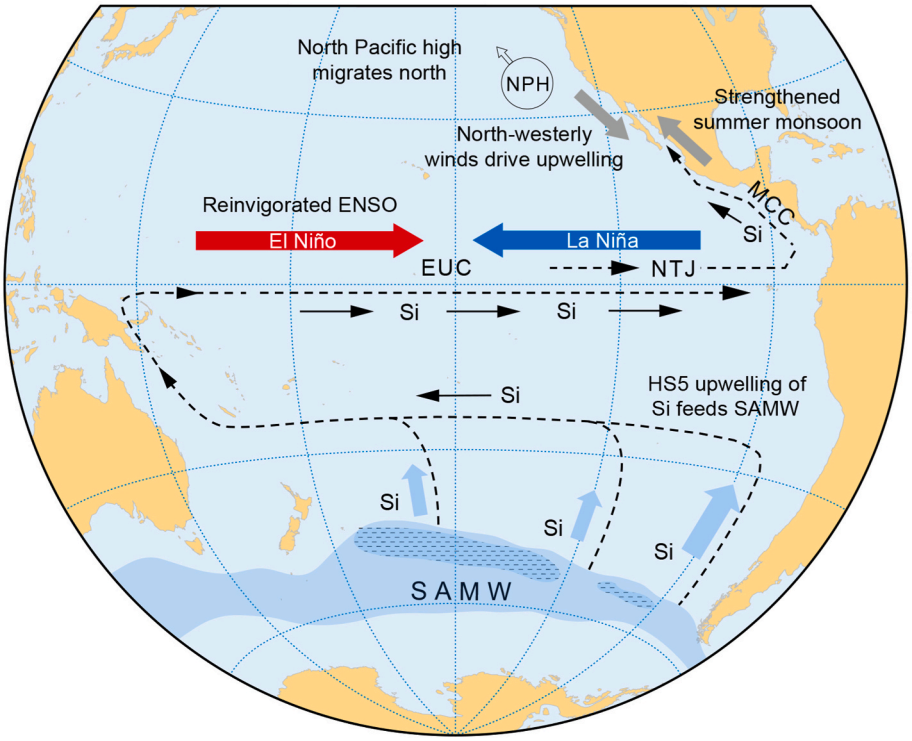


**Fig. 12.** Illustration of major changes affecting the Gulf during the transition from Henrich Stadial 5 (HS5) to Greenland Interstadial 12 (GI-12). During HS5, Southern Hemisphere warming via the bipolar seesaw results in a southward migration of the westerlies. Consequent intensification of upwelling and ventilation in the Southern Ocean leads to the enhanced formation and northward advection of Si-rich Subantarctic Mode Water (SAMW) which passes rapidly via the EUC to the Gulf. Subsequently, Northern Hemisphere warming on the transition to GI-12 leads to a strengthened North American Monsoon, intensified northwesterly winds driving spring upwelling and reinvigorated ENSO variability. The modern ocean distribution of SAMW and zones of maximum thickness (darker shading) are taken from Talley (1999), Li et al. (2021) and Wang et al. (2022). The northward tracks of SAMW and route to the EUC are taken from Tsuchiya et al. (1989), Toggweiler et al. (1991), Herraiz-Borreguero and Rintoul (2011), Bostock et al. (2013) and Li et al. (2021). Abbreviations of ocean currents are as for Fig. 2.

warming events, winter winds across the Gulf were likely from the southeast (Bartlein et al., 1998).

#### 5.1.7. *Interannual variability from lamina time series shows strengthening El Niño in the interstadial*

Examination of the lamina time series and spectral analysis (Fig. 10) reveals distinct periodicities that may be linked to time scales of known interannual variability. Concentrating on peaks above the 95% confidence level, the total diatom ooze thickness per varve (a measure of total production and flux) for the lower segment has a quasi-biennial 2.4 year peak that may be related to the quasi-biennial component of El Niño. The strongest peak at 8 years is in the top segment and this is consistent with the other evidence for the strengthening of El Niño in the interstadial. At 8 years, this is a little higher than the "classical ENSO" 3–7 year band of Allan (2000) and nearer the return interval for strong El Niño events of 8.8 years (Enfield and Cid, 1991).

The total lithogenic lamina thickness per varve is expected to relate to the intensity of monsoonal run-off and/or aeolian deposition which will be related to the monsoonal strength. The strongest peaks in the middle and top laminated segment are within the quasi-biennial band. In fact, this periodicity is widely observed within monsoon systems globally (Cai et al., 2019). Analysis of the variability in the number of *A. nodulifera* laminae per varve show "normal" El Niño periodicities (3.5 and 3 years) for the lower and middle laminated segments with both quasi-biennial and longer periodicities (7 years) for the top laminated segment, again consistent with stronger El Niño events in the full interstadial.

### 5.2. *Palaeoceanographic and palaeoclimatic synthesis*

#### 5.2.1. *Where did the silica come from: Southern Ocean source and relation to Heinrich Stadial 5*

The broader elevation in opal content in core MD02-2515 between about 53 and 40 ka (Pichevin et al., 2012) (Fig. 4) is consistent with records of biogenic opal variability from the eastern equatorial Pacific that show a broad maximum between 60 and 35 ka referred to as the Marine Isotope Stage (MIS) 3 opal peak (Dubois et al., 2010; Hayes et al., 2011; Kienast et al., 2006). Dubois et al. (2010) speculated that this opal maximum was a preservation effect, but this argument was rejected by Hayes et al. (2011) who saw a coincident minimum in $\delta^{13}C$ as evidence of increased supply of nutrient-rich deep waters to the EUC. While the broad 50 ka opal peak is present in the eastern equatorial Pacific, it is absent from the central equatorial Pacific leading Hayes et al. (2011) to propose enhanced Si supply but without enhancement of equatorial upwelling. Interestingly, the increased presence of *A. nodulifera* in the Gulf in MIS 3 between 55 and 27 ka noted by Barron et al. (2014) broadly coincides with elevated opal.

Superimposed on the broad MIS 3 opal maximum is a higher frequency multi-millenial, variability with more discrete peaks in opal flux (Dubois et al., 2011; Pichevin et al., 2012; Chang et al., 2015) culminating in the peak value of the entire MD02-2515 record at 59.6% biogenic silica (Fig. 4). The amount of silica in the EUC source of equatorial upwelling is tightly coupled to its delivery from the Southern Ocean via Subantarctic Mode Water (SAMW) (Sarmiento et al., 2004; Toggweiler et al., 1991). Increased deep ocean ventilation and upwelling of Si-rich waters around Antarctica at the last deglaciation drove increased circum-Antarctic diatom productivity and opal flux, and also resulted in enhanced supply of silica to SAMW and thence to the eastern equatorial Pacific giving increased diatom productivity and opal flux

**Table 3**
Summary of Major climate events and effects in the Gulf of California.

| Climate event/state | Atmosphere/Ocean response | Response in Gulf of California |
|---|---|---|
| **Greenland Stadial 13/ Heinrich Stadial 5** Southern Ocean surface warming via bipolar seesaw | Poleward shift of westerlies leads to enhanced Southern Ocean ventilation and Si input to Subantarctic Mode Water: this advects northwards to the Equatorial Undercurrent over 300–400 years and hence via the Mexican Coastal Current to the Gulf | Generates peak silica supply to Gulf lagged by several decades to a few centuries, favouring diatom growth and subsequent peak Si-rich sedimentation culminating in early GI-12 |
| **Greenland Interstadial 12** Retreat of Laurentide Ice Sheet to minimum extent | Reduced N-S temperature gradient leads to decline in westerlies and reinvigoration of the North American Monsoon<br>Strengthened El Niño - La Niña cyclicity<br>• During El Niño - Increased penetration of tropical Pacific waters into Gulf<br>• During La Niña – Spring upwelling enhanced | Intensified and repeated summer season Gulf Surge storms generate multiple summer flux events from recurring blooms of *Azpeitia nodulifer* diatoms<br>• Brings oceanic *Azpeitia* populations into Gulf to become dominant summer bloom species<br>• Enhances delivery of Si-rich waters to Gulf<br>• Drives *Chaetoceros* production and flux |

there also (Anderson et al., 2009). Similar peaks in circum-Antarctic opal flux driven by upwelling and ventilation occur during the Heinrich Stadials of the last glaciation, including HS5 (Gottschalk et al., 2016). Recent syntheses demonstrate that the strongest Southern Ocean ventilation episodes were triggered by the largest weakenings in the Atlantic Meridional Overturing Circulation coinciding with the strongest of the Heinrich Stadials including HS5 (Henry et al., 2016; Yu et al., 2023). These strong ventilation episodes would also have led to enhanced Si-rich SAMW formation and northward advection to the equatorial Pacific.

Chang et al. (2015) remarked on the lack of correlation of the MD02-2515 opal and $\delta^{15}N$ records with Dansgaard-Oeschger oscillations in the older part of the record, but they were using the earlier Greenland GISP2 ice core chronology of Stuiver and Grootes (2000) which has the onset of GI-12 at ~ 45,400 b2k. Here, we use the updated chronology of the NGRIP GICC05 (Svensson et al., 2008) as adopted by the INTIMATE event stratigraphy of Rasmussen et al. (2014) giving the onset of GI-12 at 46,860 b2k which is only about 400 years earlier than the radiocarbon date 2 cm from the top of our study interval at 46,418 Calendar age which is equivalent to 46,468 b2k. Using this chronology, it is feasible to relate variability in the Gulf of California more precisely to the major ocean/climate changes during HS5 and the transition to Greenland Interstadial 12 (Table 3; Fig. 12).

The synthesis of Yu et al. (2023) confirms strong Southern Ocean ventilation during HS5 within GS-13. Weakening of the Atlantic Meridional Overturing Circulation (AMOC) and north Atlantic regional cooling at the onset of HS5 (~48,137 b2k) led to Antarctic warming with a lag of around 200 years via the bipolar seesaw mechanism (WAIS Divide Members, 2015; Rhodes et al., 2015; Buizert et al., 2018). Surface warming of the Southern Ocean was accompanied by a poleward shift and strengthening of the southern westerlies leading to enhanced ventilation around Antarctica (Yu et al., 2023) and a pulse of silica-rich SAMW which then advected northwards (Fig. 12). Model simulations of the modern oceans suggest a rapid transit time, with Rodgers et al. (2003) giving an interval of ~270 years for SAMW to substantively reach the Equatorial Undercurrent (EUC) and Zuo et al. (2012) estimating as little as 50 years for this passage. The silica-rich equatorial waters would then have been delivered to the eastern tropical Pacific by the EUC and its offshoot the Northern Tsuchiya Jet and thence to the Gulf via the Mexican Coastal Current (Figs. 2 and 12). These tropical ocean waters evidently also contained the seed populations of *A. nodulifera*, leading to the exceptional diatom blooms. Increased penetration of tropical waters into the Gulf is also documented in other interstadials including the Bølling-Ållerød (Velázquez-Aguilar et al., 2024).

The ~20 wt % increase to maximum biogenic opal values in the MD02-2515 record starts during the middle varve segment (Fig. 4) and peaks at the top value of 59.6% in the top varve segment (Fig. 4). It is likely that this increase reflects the delivery of the newly Si-enriched thermocline waters to the Gulf, and this coincides with the transition from *Coscinodiscus*-dominated laminae to exclusively *A. nodulifera*-dominated laminae, also indicating the enhanced influx of oceanic waters. As well as an increase to peak opal values there is also a marked increase in nitrogen isotope ratios from $\delta^{15}N$ values of 8.3 ‰ to 11.1 ‰ (Chang et al., 2015) (Fig. 4). This follows a general pattern in Gulf sediments of elevated opal content coinciding with enrichment in $\delta^{15}N$ and is thought to relate to denitrification occurring during episodes of reduced oxygenation and lamina preservation (Pride et al., 1999).

### 5.2.2. *Intensification of the North American monsoon (NAM) on the transition to GI-12*

We interpret the multiple summer *A. nodulifera* laminae flux events in the top varve segment to be due to repeated intense Gulf surge storms that disrupted the subsurface bloom niche, temporarily destroying the thermocline resulting in mass diatom sedimentation (Fig. 11). Uncertainties in the age model notwithstanding, the top laminated segment is nearest to the peak interstadial. This is consistent with the increased NAM intensity to be expected with GI-12 Interstadial Northern Hemisphere warming (Fig. 12).

In general, there is an anti-phased, inter-hemispheric relationship between the Northern and Southern Hemisphere monsoon systems with the Northern monsoons weakening during episodes of Northern Hemisphere cooling on timescales from orbital to millennial to centennial (Cheng et al., 2012). More specifically, during Greenland Interstadials, the ITCZ shifted northward, and the Indian and East Asian Monsoons strengthened (Deplazes et al., 2014; Izumi et al., 2023). While there is no data on the North American Monsoon for the earlier Greenland Interstadials, it likely followed the same Northern Hemisphere monsoon pattern as it did during the more recent, with collapse during DO cold intervals – Heinrich Stadial 1 (HS1 or GS-2) and Younger Dryas (GS-1) and resurgence with early Holocene warming (Lachniet et al., 2013). Significantly, the stronger Heinrich DO cycles are associated with greater amplitude change in the global monsoon systems (Dong et al., 2022). The temperature rise at the NGRIP site at the onset of GI-12, at 12.5 °C was one of the stronger rises recorded at the GI onsets (Kindler et al., 2014) and a relatively swift transition with a duration of ~60 years (Erhardt et al., 2019), so the strengthening of the NAM was likely vigorous and rapid.

Recent analyses of NAM behaviour place more emphasis on atmospheric circulation changes linked to latitudinal temperature gradients relating to the size of the Laurentide ice sheet rather than the ITCZ influences, with ice sheet decline in concert with increasing NAM monsoon strength (Bhattacharya et al., 2017; Routson et al., 2022). In periods of increased Laurentide ice sheet extent, the stronger westerlies promoted by stronger latitudinal temperature gradients suppress the NAM by blocking anticyclone development and northward progression. As the Laurentide ice sheet declined following the last Glacial Maximum, so the westerlies decreased in strength, allowing the monsoon to

reinvigorate (Bhattacharya et al., 2018; Routson et al., 2022), and a similar pattern may be hypothesized for the transition to the warmest interstadials. Although there are dating uncertainties, the reconstructed Laurentide Ice Sheet for 45 kyr (Batchelor et al., 2019; Dalton et al., 2022) shows a minimum MIS 3 configuration similar in extent to that at ~ 8.5 ka (Dalton et al., 2020). The ice rafted detritus of HS5 was derived from the Hudson Straight, consistent with purging of the Laurentide Ice Sheet immediately prior to the onset of GI 12 (Hemming, 2004). This would then lead to declining westerlies and a strengthened NAM at GI 12. This is also consistent with our evidence for strengthened El Niño/La Niña cyclicity in the Interstadial, since model simulations show abrupt intensification of ENSO forced by Laurentide Ice Sheet retreat (Lu et al., 2016).

#### 5.2.3. Increasing *A. nodulifera* dominance indicates strong El Niño activity

*A. nodulifera* becomes increasingly dominant upwards through the laminated segments, displacing large *Coscinodiscus* spp. in the annual flux cycle. From the known association of *A. nodulifera* with tropical waters and El Niño events in the Gulf, it is likely that these increased abundances reflect increased penetration of tropical waters into the Gulf through the interval, with peak penetration at the full interstadial (top laminated segment). Records from the last glacial cycle show a dampening of El Niño during cold intervals with a resurgence in warm intervals (Tudhope et al., 2001) and there is evidence that El Niño activity increased during DO Interstadials (Turney et al., 2004). Furthermore, annually resolved reconstructions from giant clams demonstrate strong El Niño variability during MIS 3 (Driscoll et al., 2014). The strong Kelvin wave activity generated by the El Niño events would have intensified the poleward Mexican Coastal Current, so enhancing the delivery of the Si-rich sub-thermocline tropical waters to the Gulf thus further boosting diatom productivity.

Evidence for strengthened El Niño activity in the transition to the interstadial is also provided by the results of the time series analysis (Fig. 10) that show the strongest peaks in the ENSO band occurring in the top laminated segment.

#### 5.2.4. Alternations of *A. nodulifera* – and *Chaetoceros setae* - dominated varves represent El Niño/La Niña cyclicity

Our observations of 2-to-3-year alternations between *A. nodulifera*-dominated varves and *Chaetoceros setae* – dominated varves indicate alternations of years with production and flux mainly in stratified waters with years when production was mainly driven by upwelling. These results are consistent with analyses of modern El Niño/La Niña cyclicity that shows multi-year La Niña states are generally preceded by strong El Niño events that themselves are commonly of a two-year duration (Iwakiri and Watanabe, 2021). During strong El Niño winters the thermocline is deepened, and upwelling winds are suppressed resulting in much reduced upwelling production. On the other hand, during La Niña summers, SST are reduced resulting in weakened stratification and atmospheric convection is inhibited resulting in weaker/fewer monsoonal storms (see references and discussion in 2.1.2).

## 6. Conclusions

Reconstruction of a "paleo-sediment trap" varved sediment record from the Gulf of California that spans that transition from Heinrich Stadial 5 (HS5, Greenland Stadial 13) to Greenland Interstadial 12, has documented superbly preserved and exceptional blooms of the large tropical oceanic diatom *Azpeitia nodulifera*. These events record the influx of eastern tropical Pacific waters to the Gulf likely associated with strong El Niño activity. Hitherto not thought to be a "bloom species", *A. nodulifera* was able to grow at depth in stratified waters exploiting deep (nutricline) nutrient sources. The sedimentation of actively blooming populations is indicated by the presence of 60% of cells in the process of vegetative division that show every stage in the cell division cycle.

The *A. nodulifera* bloom deposits represent the most opal-rich concentrations of the entire 55 kyr MD02-2515 core at 59.6% biogenic silica. The silica-rich waters were likely sourced from increased production of Subantarctic Mode Water in response to Southern Hemisphere warming during Heinrich Stadial 5 within Greenland Stadial 13, via the bipolar seesaw mechanism. These silica-rich waters were rapidly supplied to the Equatorial Undercurrent and the associated North Tsuchiya Jet and thence to the Mexican Coastal Current feeding directly to the Gulf. The sequence also records the strengthening of El Niño and resurgence of the North American Monsoon on Northern Hemisphere warming in the transition to Greenland Interstadial 12. A strengthened El Niño aided penetration of tropical ocean waters to the Gulf bringing the seed populations of *A. nodulifera* and enhancing water column stratification to which the diatoms were adapted by the ability to grow at depth in low light conditions, likely at the nutricline. Multiple flux events of *A. nodulifera* blooms in any given year, suggest the enhanced and repeated incidence of strong monsoonal Gulf surge storms that disrupted the water column stratification and caused the blooms to sediment. The persistence of sufficient nutrients and diatom seed populations led to renewed blooms on the resumption of stratification after the Gulf surge storms. Abundant *Chaetoceros* spp. diatoms in the youngest, Interstadial laminated interval record renewed vigour of winter – spring upwelling associated with the strengthening of northwesterly winds as the north Pacific high migrated northwards. Alternations between *A. nodulifera* -dominated years and years with abundant *Chaetoceros* spp. suggest an alternation between strong El Niño and La Niña on 2–3 year timescales. The monsoon intensification, the resurgence in El Niño strength and the strengthened winter-spring northwesterlies were likely all driven by the climatic response to reduction to a minimum extent of the Laurentide Ice Sheet in Greenland Interstadial 12.

This study adds to an increasing body of evidence that diatom taxa adapted to stratified conditions, and previously thought not significant producers, may bloom to produce water column and sediment concentrations comparable to those typical of the spring bloom or upwelling pulse. The climatic changes in the Gulf in the transition to the warm Interstadial may serve as a pointer to possible future changes in the Gulf driven by the present warming trend.

## CRediT authorship contribution statement

**Helen Griffin:** Writing – review & editing, Writing – original draft, Methodology, Investigation, Formal analysis, Data curation, Conceptualization. **Alan E.S. Kemp:** Writing – review & editing, Writing – original draft, Methodology, Supervision, Project administration, Investigation, Formal analysis, Conceptualization, Funding acquisition. **Richard B. Pearce:** Writing – review & editing, Investigation, Methodology, Supervision, Formal analysis.

## Declaration of competing interest

The authors declare that they have no known competing financial interests or personal relationships that could have appeared to influence the work reported in this paper.

## Data availability

Data will be made available on request.

## Acknowledgements

The research was supported by the Natural Environment Research Council (UK) (grant number NE/C520412/1) to A.E.S.K. and a NERC Research Studentship to H.G. We thank the IMAGES IV Programme and the crew and scientific party of the MONA expedition (R/V *Marion Dufresne*) for core collection. We are grateful to Juergen Thurow for discussions and comments on an earlier version of the manuscript, to

Heiko Palike for advice on time series analysis and to Alberto Naveira Garabato for discussions on Subantarctic Mode Water. Kate Davis is thanked for drafting expertise.

## References


Adams, D.K., Comrie, A.C., 1997. The North American monsoon. Bull. Am. Meteorol. Soc. 78, 2917, 2213.

Allan, R.J., 2000. ENSO and climatic variability in the past 150 years. In: Diaz, H.F., Markgraf, V. (Eds.), El Nino and the Southern Oscillation. Cambridge University Press, pp. 3–55.

Alldredge, A.L., Goltschalk, C.G., 1989. Direct observations of the mass floculation of diatom blooms: characteristics, settling velocities and formation of diatom aggregates. Deep-Sea Res. I 36, 159–171.

Anderson, R.F., Ali, S., Bradtmiller, L.I., Nielsen, S.H.H., Fleisher, M.Q., Anderson, B.E., Burkle, L.H., 2009. Wind-driven upwelling in the Southern Ocean and the deglacial rise in atmospheric $CO_2$. Science 323, 1443–1448.

Badan-Dangon, A., Dorman, C.E., Merrifield, M.A., Winant, C.D., 1991. The lower atmosphere over the gulf of California. J. Geophys. Res. 96, 877–896.

Badan-Dangon, A., Koblinsky, C.J., Baumgartner, T.R., 1985. Spring and summer in the Gulf of California: observations of surface thermal patterns. Oceanol. Acta 8.

Barron, J.A., 2003. Planktonic marine diatom record of the past 18 M.y.: appearances and extinction in the Pacific and Southern Oceans. Diatom Res. 18, 203–224.

Barron, J.A., Bukry, D., 2007. Solar forcing of Gulf of California climate during the past 2000kyr suggested by diatoms and silicoflagellates. Mar. Micropaleontol. 62, 115–139.

Barron, J.A., Bukry, D., Bischoff, J.L., 2004. High resolution paleoceanography of the Guaymas Basin, Gulf of California, during the past 15 000 years. Mar. Micropaleontol. 50, 185–207.

Barron, J.A., Bukry, D., Chesire, H., 2014. Response of diatom and silicoflagellate assemblages in the central Gulf of California to regional climate change during the past 55 kyrs. Mar. Micropaleontol. 108, 28–40.

Barron, J.A., Bukry, D., Dean, W.E., 2005. Paleoceanographic history of the Guaymas Basin, Gulf of California, during the past 15,000 years based on diatoms, silicoflagellates, and biogenic sediments. Mar. Micropaleontol. 56, 81–102.

Bartlein, P.J., Anderson, K.H., Anderson, P.M., Edwards, M.E., Mock, C.J., Thompson, R. S., Webb, R.S., Whitlock, C., 1998. Paleoclimate simulations for North America over the past 21,000 years: features of the simulated climate and comparisons with paleoenvironmental data. Quat. Sci. Rev. 17, 549–585.

Batchelor, C.L., Margold, M., Krapp, M., Murton, D., Dalton, A.S., Gibbard, P.L., Stokes, C.R., Murton, J.B., Manica, A., 2019. The configuration of Northern Hemisphere ice sheets through the Quaternary. Nat. Commun. 10, 3713. https://doi.org/10.1038/s41467-019-11601-2.

Baumgartner, T.R., Christensen, N., 1985. Coupling of the Gulf of California to large-scale interannual climatic variability. J. Mar. Res. 43, 825–848.

Baumgartner, T.R., Ferreira-Bartrina, V., Moreno-Hentz, P., 1991. Varve formation in the central Gulf of California: a reconsideration of the origin of the dark laminae from the 20th Century varve record. In: Dauphin, J.P., Simoneit, B.R.T. (Eds.), The Gulf and Peninsular Province of the Californias. American Association of Petroleum Geologists, Tulsa, pp. 617–635.

Baumgartner, T.R., Ferreira-Bartrina, V., Schrader, H., Soutar, A., 1985. A 20-year varve record of siliceous phytoplankton variability in the central Gulf of California. Mar. Geol. 64, 113–129.

Beaufort, L., the Members of the Scientific Party, 2002. Cruise Report, MD 126, MONA IMAGES VIII. Inst. Polaire Français Paul-Emile Victor, Plouzané, France, p. 453.

Bhattacharya, T., Chiang, J.C.H., 2014. Spatial variability and mechanisms underlying El Nino-induced droughts in Mexico. Clim. Dynam. 43, 3309–3326.

Bhattacharya, T., Tierney, J.E., Addison, J.A., Murray, J.W., 2018. Ice-sheet modulation of deglacial North American monsoon intensification. Nat. Geosci. 11, 848–852. https://doi.org/10.1038/s41561-018-0220-7.

Bhattacharya, T., Tierney, J.E., DiNezio, P., 2017. Glacial reduction of the North American Monsoon via surface cooling and atmospheric ventilation. Geophys. Res. Lett. 44, 5113–5122.

Billett, D.S.M., Lampitt, R.S., Rice, A.L., Mantoura, R.F.C., 1983. Seasonal sedimentation of phytoplankton to the deep-sea benthos. Nature 302, 520–522.

Bordoni, S., Ciesielski, P.E., Johnson, R.H., McNoldy, B.D., Stevens, B., 2004. The low-level circulation of the North American Monsoon as revealed by QuikSCAT. Geophys. Res. Lett. 31. https://doi10.1029/2004gl020009.

Bordoni, S., Stevens, B., 2006. Principal component analysis of the summertime winds over the Gulf of California: a Gulf surge index. Mon. Weather Rev. 134, 3395–3414.

Bostock, H.C., Sutton, P.J., Williams, M.J.M., Opdyke, B.N., 2013. Reviewing the circulation and mixing of Antarctic Intermediate Water in the South Pacific using evidence from geochemical tracers and Argo float trajectories. Deep-Sea Res. I 73, 84–98.

Bray, N.A., Robles, J.M., 1991. Physical oceanography of the gulf of California. In: Dauphin, J.P., Simoneit, B.R.T. (Eds.), The Gulf and Peninsular Province of the Californias, vol. 47. American Association of Petroleum Geologists, Memoir, pp. 511–553.

Brodie, I., Kemp, A.E.S., 1994. Variation in biogenic and detrital fluxes and formation of laminae in late Quaternary sediments from the Peruvian coastal upwelling zone. Mar. Geol. 116, 385–398.

Bromble, S.L., Burckle, L.H., 1983. A late quaternary stratigraphy for DSDP site 480, gulf of California. Mar. Micropaleontol. 7, 541–543.

Buizert, C., Sigl, M., Severi, M., Marckle, B.R., Wettstein, J.J., McConnell, J.R., Pedro, J. B., Sodemann, H., Goto-Azuma, K., Kawamura, K., Fujita, S., Motoyama, H., Hirabayashi, M., Uemura, R., Stenni, B., Parrenin, F., He, F., Fudge, T.J., Steig, E.J., 2018. Abrupt ice-age shifts in southern westerly winds and Antarctic climate forced from the north. Nature 563, 681–685.

Bull, D., Kemp, A.E.S., Weedon, G.P., 2000. A 160-k.y.-old record of El Niño-Southern Oscillation in marine production and coastal runoff from Santa Barbara Basin, California, USA. Geology 28, 1007–1010.

Burckle, L.H., McLaughlin, R.B., 1977. Size changes in the marine diatom *Coscinodiscus nodulifer* A. Schmidt in the equatorial Pacific. Micropaleontology 23, 216–222.

Burckle, L.H., Shackleton, N.J., Bromble, S.L., 1981. Late quaternary stratigraphy for the equatorial pacific based upon the diatom Coscinodiscus nodulifer. Micropaleontology 27, 352–355.

Cai, J.X., Xu, J.J., Guan, Z.Y., Powell, A.M., 2019. Interdecadal variability of El Nino onset and its impact on monsoon systems over areas encircling the Pacific Ocean. Clim. Dynam. 52, 7173–7188.

Calvert, S.E., 1966. Origin of diatom-rich varved sediments from the Gulf of California. J. Geol. 74, 546–565.

Castro, C.L., McKee, T.B., Pielke, R.A., 2001. The relationship of the North American monsoon to tropical and North Pacific Sea surface temperatures as revealed by observational analyses. J. Clim. 14, 4449–4473.

Chang, A.S., Patterson, T.R., McNeely, R., 2003. Seasonal sediment and diatom record from late Holocene laminated sediments, effingham inlet, British columbia, Canada. Palaios 18, 477–494.

Chang, A.S., Pichevin, L., Pedersen, T.F., Gray, V., Ganeshram, R., 2015. New insights into productivity and redox-controlled trace element (Ag, Cd, Re, and Mo) accumulation in a 55kyr long sediment record from Guaymas Basin, Gulf of California. Paleoceanography 30, 77–94.

Cheng, H., Sinha, A., Wang, X.F., Cruz, F.W., Edwards, R.L., 2012. The global paleomonsoon as seen through speleothem records from asia and the americas. Clim. Dynam. 39, 1045–1062.

Cheshire, H., Thurow, J., 2013. High-resolution migration history of the Subtropical High/Trade Wind system of the northeastern Pacific during the last ~55 years: implications for glacial atmospheric reorganization. Paleoceanography 28, 319–333.

Crawford, R.M., 1995. The role of sex in the sedimentation of a marine diatom bloom. Limnol. Oceanogr. 40, 200–204.

Dalton, A.S., Margold, M., Stokes, C.R., Tarasov, L., Dyke, A.S., Adams, R.S., Allard, S., Arends, H.E., Atkinson, N., Attig, J.W., Barnett, P.J., Barnett, R.L., Batterson, M., Bernatchez, P., Borns, H.W., Breckenridge, A., Briner, J.P., Brouard, E., Campbell, J. E., Carlson, A.E., Clague, J.J., Curry, B.B., Daigneault, R.A., Dube-Loubert, H., Easterbrook, D.J., Franzi, D.A., Friedrich, H.G., Funder, S., Gauthier, M.S., Gowan, A.S., Harris, K.L., Hetu, B., Hooyer, T.S., Jennings, C.E., Johnson, M.D., Kehew, A.E., Kelley, S.E., Kerr, D., King, E.L., Kjeldsen, K.K., Knaeble, A.R., Lajeunesse, P., Lakeman, T.R., Lamothe, M., Larson, P., Lavoie, M., Loope, H.M., Lowell, T.V., Lusardi, B.A., Manz, L., McMartin, I., Nixon, F.C., Occhietti, S., Parkhill, M.A., Piper, D.J.W., Pronk, A.G., Richard, P.J.H., Ridge, J.C., Ross, M., Roy, M., Seaman, A., Shaw, J., Stea, R.R., Teller, J.T., Thompson, W.B., Thorleifson, L.H., Utting, D.J., Veillette, J.J., Ward, B.C., Weddle, T.K., Wright, H.E., 2020. An updated radiocarbon-based ice margin chronology for the last deglaciation of the North American Ice Sheet Complex. Quat. Sci. Rev. 234, 106223 https://doi.org/10.1016/j.quascirev.2020.106223.

Dalton, A.S., Stokes, C.R., Batchelor, C.L., 2022. Evolution of the Laurentide and innuitian ice sheets prior to the last glacial maximum (115 ka to 25 ka). Earth Sci. Rev. 224, 103875.

Davies, A., Kemp, A.E.S., Weedon, G.P., Barron, J.A., 2012. El niño-southern oscillation variability from the late cretaceous marca shale of California. Geology 40, 15–18.

Dean, J.M., Kemp, A.E.S., Bull, D., Pike, J., Patterson, G., Zolitschka, B., 1999. Taking varves to bits: scanning electron microscopy in the study of laminated sediments and varves. J. Paleolimnol. 22, 121–136.

Dean, J.M., Kemp, A.E.S., Pearce, R.B., 2001. Palaeo-flux records from electron microscope studies of Holocene laminated sediments. Saanich Inlet, British Columbia. Mar Geol 174, 139–158.

Deplazes, G., Luckge, A., Stuut, J.B.W., Patzold, J., Kuhlmann, H., Husson, D., Fant, M., Haug, G.H., 2014. Weakening and strengthening of the Indian monsoon during Heinrich events and Dansgaard- Oeschger oscillations. Paleoceanography 29, 99–114.

Devries, T.J., Schrader, H., 1981. Variation of upwelling-oceanic conditions during the latest Pleistocene through Holocene off the central Peruvian coast - a diatom record. Mar. Micropaleontol. 6, 157–167.

Donegan, D., Schrader, H., 1982. Biogenic and abiogenic components of laminated hemipelagic sediments in the central Gulf of California. Mar. Geol. 48, 215–237.

Dong, X.Y., Kathayat, G., Rasmussen, S.O., Svensson, A., Severinghaus, J.P., Li, H.Y., Sinha, A., Xu, Y., Zhang, H.W., Shi, Z.G., Cai, Y.J., Perez-Mejias, C., Baker, J., Zhao, J.Y., Spotl, C., Columbu, A., Ning, Y.F., Strikis, N.M., Chen, S.T., Wang, X.F., Gupta, A.K., Dutt, S., Zhang, F., Cruz, F.W., An, Z.S., Edwards, R.L., Cheng, H., 2022. Coupled atmosphere-ice-ocean dynamics during Heinrich stadial 2. Nat. Commun. 13, 5867. https://doi.org/10.1038/s41467-022-33583-4.

Douglas, M.W., Li, S.H., 1996. Diurnal variation of the lower-tropospheric flow over the Arizona low desert from SWAMP-1993 observations. Mon. Weather Rev. 124, 1211–1224.

Douglas, R., Gonzalez-Yajimovich, O., Ledesma-Vazquez, J., Staines-Urias, F., 2007. Climate forcing, primary production and the distribution of Holocene biogenic sediments in the Gulf of California. Quat. Sci. Rev. 26, 115–129.

Driscoll, R., Elliot, M., Russon, T., Welsh, K., Yokoyama, Y., Tudhope, A., 2014. ENSO reconstructions over the past 60 ka using giant clams (Tridacna sp.) from Papua New Guinea. Geophys. Res. Lett. 41, 6819–6825.

Dubois, N., Kienast, M., Kienast, S., Calvert, S.E., Francois, R., Anderson, R.F., 2010. Sedimentary opal records in the eastern equatorial Pacific: it is not all about leakage. Global Geochemical Cycles 24 (10). https://doi.org/10.1029/2010GB003821.
Dubois, N., Kienast, M., Kienast, S., Normandeau, C., Calvert, S.E., Herbert, T.D., Mix, A., 2011. Millennial-scale variations in hydrography and biogeochemistry in the Eastern Equatorial Pacific over the last 100 kyr. Quat. Sci. Rev. 30, 210–223.
Enfield, D., Cid, L., 1991. Low-frequency changes in El niño-southern oscillation. J. Clim. 4, 1137–1146.
Erhardt, T., Capron, E., Rasmussen, S.O., Schupbach, S., Bigler, M., Adolphi, F., Fischer, H., 2019. Decadal-scale progression of the onset of Dansgaard-Oeschger warming events. Clim. Past 15, 811–825.
Francus, P., Keimig, F., Besonen, M., 2002. An algorithm to aid varve counting and measurement from thin-sections. J. Paleolimnol. 28, 283–286.
Fryxell, G.A., Sims, P.A., Watkins, T.P., 1986. Azpeitia (bacillariophyceae): related genera and promorphology. Systematic Botany Monographs 13, 1–74.
Fuller, R.D., Stensrud, D.J., 2000. The relationship between tropical easterly waves and surges over the Gulf of California during the North American monsoon. Mon. Weather Rev. 128, 2983–2989.
Garcia-Morales, R., Lopez-Martinez, J., Valdez-Holguin, J.E., Herrera-Cervantes, H., Espinosa-Chaurand, L.D., 2017. Environmental variability and oceanographic dynamics of the central and southern coastal zone of Sonora in the gulf of California. Rem. Sens. 9, 925. https://doi.org/10.3390/rs9090925.
Godinez, V.M., Beier, E., Lavìn, M.F., Kurczyn, J.A., 2010. Circulation at the entrance of the Gulf of California from satellite altimeter and hydrographic observations. J. Geophys. Res. 115, C04007.
Goldman, J.C., 1993. Potential role of large oceanic diatoms in new primary production. Deep-Sea Res. I 40, 159–168.
Goldman, J.C., McGillicuddy, D.G.J., 2003. Effect of large marine diatoms growing at low light on episodic new production. Limnol. Oceanogr. 48, 1176–1182.
Gomez-Valdivia, F., Pares-Sierra, A., Flores-Morales, A.L., 2015. The Mexican Coastal Current: a subsurface seasonal bridge that connects the tropical and subtropical Northeastern Pacific. Continent. Shelf Res. 110, 100–107.
Gottschalk, J., Skinner, L.C., Lippold, J., Vogel, H., Frank, N., Jaccard, S.L., Waelbroeck, C., 2016. Biological and physical controls in the Southern Ocean on past millennial-scale atmospheric $CO_2$ changes. Nat. Commun. 7, 11539 https://doi.org/10.1038/ncomms11539.
Grimm, K.A., Lange, C.B., Gill, A.S., 1997. Self-sedimentation of phytoplankton blooms in the geological record. Sediment. Geol. 110, 151–161.
Hayes, C.T., Anderson, R.F., Fleisher, M.Q., 2011. Opal accumulation rates in the equatorial Pacific and mechanisms of deglaciation. Paleoceanography 26 (1). https://doi.org/10.1029/2010PA002008.
Hemming, S.R., 2004. Heinrich events: massive Late Pleistocene detritus layers of the North Atlantic and their global climate imprint. Rev. Geophys. 42, RG1005 https://doi.org/10.1029/2003RG000128.
Henry, L.G., McManus, J.F., Curry, W.B., Roberts, N.L., Piotrowski, A.M., Keigwin, L.D., 2016. North Atlantic ocean circulation and abrupt climate change during the last glaciation. Science 353, 470–474.
Herraiz-Borreguero, L., Rintoul, S.R., 2011. Subantarctic mode water: distribution and circulation. Ocean Dynam. 61, 103–126.
Herrera-Cervantes, H., Lluch-Cota, D.B., Lluch-Cota, S.E., Guillermo, G.D.V.S., 2007. The ENSO signature in sea-surface temperature in the Gulf of California. J. Mar. Res. 65, 589–605.
Higgins, R.W., Chen, Y., Douglas, A.V., 1999. Interannual variability of the North American warm season precipitation regime. J. Clim. 12, 653–680.
Higgins, R.W., Shi, W., 2001. Intercomparison of the principal modes of interannual and intraseasonal variability of the North American Monsoon System. J. Clim. 14, 403–417.
Higgins, R.W., Shi, W., 2005. Relationships between Gulf of California moisture surges and tropical cyclones in the eastern Pacific basin. J. Clim. 18, 4601–4620.
Hu, Q., Feng, S., 2008. Variation of the North American summer monsoon regimes and the Atlantic multidecadal oscillation. J. Clim. 21, 2371–2383.
Idso, S.B., 1976. Chubasco. Weather 31, 224–226.
Iriarte, J.L., Fryxell, G.A., 1995. Micro-phytoplankton at the equatorial pacific (140-degrees-W) during the JGOFS EqPac time-series studies - march to April and october 1992. Deep-Sea Research Pt II 42, 559–583.
Iwakiri, T., Watanabe, M., 2021. Mechanisms linking multi-year La Nina with preceding strong El Nino. Sci. Rep. 11, 17465 https://doi.org/10.1038/s41598-021-96056-6.
Izumi, K., Armstrong, E., Valdes, P., 2023. Global footprints of dansgaard-oeschger oscillations in a GCM. Quat. Sci. Rev. 305, 108016 https://doi.org/10.1016/j.quascirev.2023.108016.
Kahru, M., Marinone, S.G., Lluch-Cota, S.E., Pares-Sierra, A., Mitchell, B.G., 2004. Ocean-color variability in the Gulf of California: scales from days to ENSO. Deep-Sea Research Pt II 51, 139–146.
Kalansky, J.F., Robinson, R.S., Popp, B.N., 2011. Insights into nitrogen cycling in the western Gulf of California from the nitrogen isotopic composition of diatom-bound organic matter. G-cubed 12 (6), Q06015. https://doi.org/10.1029/2010GC003437.
Kemp, A.E.S., 2003. Evidence for abrupt climate changes in annually laminated marine sediments. Philosophical Transactions of the Royal Society of London Series a-Mathematical Physical and Engineering Sciences 361, 1851–1870.
Kemp, A.E.S., Dean, J., Pearce, R.B., Pike, J., 2001. Recognition and analysis of bedding and sediment fabric features. In: Last, W.M., Smol, J.P. (Eds.), Tracking Environmental Change Using Lake Sediments. Volume 2: Physical and Geochemical Methods. Kluwer Academic Publishers, Dordrecht, pp. 7–22.
Kemp, A.E.S., Pearce, R.B., Grigorov, I., Rance, J., Lange, C.B., Quilty, P., Salter, I., 2006. Production of giant marine diatoms and their export at oceanic frontal zones: implications for Si and C flux from stratified oceans. Global Biogeochem. Cycles 20, GB4S04. https://doi.org/10.1029/2006GB002698.
Kemp, A.E.S., Pearce, R.B., Pike, J., Marshall, J.E.A., 1998. 27. Microfabric and microcompositional studies of the pliocene and quaternary sapropels from the eastern mediterranean. In: Robertson, A.H.F., Emeis, K.-C., Richter, C., Camerlenghi, A. (Eds.), Proceedings of the Ocean Drilling Program, Scientific Results, pp. 333–348. College Station TX, (Ocean Drilling Program).
Kemp, A.E.S., Pike, J., Pearce, R.B., Lange, C.B., 2000. The "Fall dump" - a new perspective on the role of a "shade flora" in the annual cycle of diatom production and export flux. Deep-Sea Research Pt II 47, 2129–2154.
Kemp, A.E.S., Villareal, T.A., 2018. The case of the diatoms and the muddled mandalas: time to recognize diatom adaptations to stratified waters. Prog. Oceanogr. 167, 138–149.
Kessler, W.S., 2006. The circulation of the eastern tropical Pacific: a review. Prog. Oceanogr. 69, 181–217.
Kienast, S.S., Kienast, M., Jaccard, S., Calvert, S.E., Francois, R., 2006. Testing the silica leakage hypothesis with sedimentary opal records from the eastern equatorial Pacific over the last 150 kyrs. Geophys. Res. Lett. 33 (15) https://doi.org/10.1029/2006GL026651.
Kindler, P., Guillevic, M., Baumgartner, M., Schwander, J., Landais, A., Leuenberger, M., 2014. Temperature reconstruction from 10 to 120 kyr b2k from the NGRIP ice core. Clim. Past 10, 887–902.
Kobayashi, F., Takahashi, K., 2002. Distribution of diatoms along the equatorial transect in the western and central Pacific during the 1999 La Nina conditions. Deep-Sea Res Pt II 49, 2801–2821.
Lachniet, M.S., Asmerom, Y., Bernal, J.P., Polyak, V.J., Vazquez-Selem, L., 2013. Orbital pacing and ocean circulation-induced collapses of the Mesoamerican monsoon over the past 22,000 y. Proc. Natl. Acad. Sci. U.S.A. 110, 9255–9260.
Lange, C.B., Berger, W.H., 1993. Diatom productivity and preservation in the western equatorial Pacific: the Quaternary record. In: Berger, W.H., Kroenke, L.W., Mayer, L. A. (Eds.), Proceedings ODP Scientific Results, pp. 509–523. College Station, TX (Ocean Drilling Program).
Lavin, M.F., Palacios-Hernandez, E., Cabrera, C., 2003. Sea surface temperature anomalies in the Gulf of California. Geofisc. Int. 42, 363–375.
Li, Z., England, M.H., Groeskamp, S., Cerovečki, I., Luo, Y., 2021. The origin and fate of subantarctic mode water in the Southern Ocean. J. Phys. Oceanogr. 59, 2951–2972.
Lluch-Cota, S.E., 2000. Coastal upwelling in the eastern Gulf of California. Oceanol. Acta 23, 731–740.
Lora, J.M., Mitchell, J.L., Tripati, A.E., 2016. Abrupt reorganization of North Pacific and western North American climate during the last deglaciation. Geophys. Res. Lett. 43, 11796–11804.
Lu, Z.Y., Liu, Z.Y., Zhu, J., 2016. Abrupt intensification of ENSO forced by deglacial ice-sheet retreat in CCSM3. Clim. Dynam. 46, 1877–1891.
McCabe-Glynn, S., Johnson, K.R., Strong, C., Berkelhammer, M., Sinha, A., Cheng, H., Edwards, R.L., 2013. Variable North pacific influence on drought in southwestern north America since AD 854. Nat. Geosci. 6, 617–621.
McClymont, E.L., Ganeshram, R.S., Pichevin, L.E., Talbot, H.M., van Dongen, B.E., Thunell, R.C., Haywood, A.M., Singarayer, J.S., Valdes, P.J., 2012. Sea-surface temperature records of Termination 1 in the Gulf of California: challenges for seasonal and interannual analogues of tropical Pacific climate change. Paleoceanography 27 (2). https://doi.org/10.1029/2011PA002226.
Mitchell, D.L., Ivanova, D., Rabin, R., Brown, T.J., Redmond, K., 2002. Gulf of California sea surface temperatures and the North American monsoon: mechanistic implications from observations. J. Clim. 15, 2261–2281.
Morales, U.R., Vasquez, B.C., Gonzalez, R.P., Austria, P.M., 2023. Influence of the AMO and its modulation of the ENSO effects on summer precipitation in Mexican coastal regions. Water Pract. Technol. 18 (2), 304–319.
Murray, D., Schrader, H., 1982. The size distribution of the centric diatom *Coscinodiscus nodulifer*, Site 480, Guaymas Basin slope, Gulf of California. In: Curray, J.R., Moore, D.G., al, e. (Eds.), Initial Reports DSDP, vol. 64. U.S. Govt. Printing Press, Washington, pp. 1239–1244.
Pascale, S., Bordoni, S., 2016. Tropical and extratropical controls of gulf of California surges and summertime precipitation over the southwestern United States. Mon. Weather Rev. 144, 2695–2718.
Pascale, S., Kapnick, S.B., Bordoni, S., Delworth, T.L., 2018. The influence of $CO_2$ forcing on north American monsoon moisture surges. J. Clim. 31, 7949–7968.
Pichevin, L., Ganeshram, R.S., Reynolds, B.C., Prahl, F., Pedersen, T.F., Thunell, R., McClymont, E.L., 2012. Silicic acid biogeochemistry in the Gulf of California: insights from sedimentary Si isotopes. Paleoceanography 27 (2). https://doi.org/10.1029/2011PA002237.
Pike, J., Kemp, A.E.S., 1996a. Records of seasonal flux in Holocene laminated sediments, Gulf of California. In: Kemp, A.E.S. (Ed.), Palaeoclimatology and Palaeoceanography from Laminated Sediments, vol. 116. Geol. Soc. Spec. Pub., London, pp. 157–169.
Pike, J., Kemp, A.E.S., 1996b. Preparation and analysis techniques for studies of laminated sediments. In: Kemp, A.E.S. (Ed.), Palaeoclimatology and Palaeoceanography from Laminated Sediments, vol. 116. Geol. Soc. Spec. Pub., London, pp. 37–48.
Pike, J., Kemp, A.E.S., 1997. Early Holocene decadal-scale ocean variability recorded in Gulf of California laminated sediments. Paleoceanography 12, 227–238.
Pokras, E.M., Molfino, B., 1986. Oceanographic control of diatom abundances and species distributions in surface sediments of the tropical and southeast Atlantic. Mar. Micropaleontol. 10, 165–188.
Pride, C., Thunell, R., Sigman, D., Keigwin, L., Altabet, M., Tappa, E., 1999. Nitrogen isotopic variations in the Gulf of California since the last deglaciation: response to global climate change. Paleoceanography 14, 397–409.

Rackebrandt, N., Kuhnert, H., Groeneveld, J., Bickert, T., 2011. Persisting maximum Agulhas leakage during MIS 14 indicated by massive Ethmodiscus oozes in the subtropical South Atlantic. Paleoceanography 26 (3). https://doi.org/10.1029/2010PA001990.

Rasmussen, S.O., Bigler, M., Blockley, S.P., Blunier, T., Buchardt, S.L., Clausen, H.B., Cvijanovic, I., Dahl-Jensen, D., Johnsen, S.J., Fischer, H., Gkinis, V., Guillevic, M., Hoek, W.Z., Lowe, J.J., Pedro, J.B., Popp, T., Seierstad, I.K., Steffensen, J.P., Svensson, A.M., Vallelonga, P., Vinther, B.M., Walker, M.J.C., Wheatley, J.J., Winstrup, M., 2014. A stratigraphic framework for abrupt climatic changes during the Last Glacial period based on three synchronized Greenland ice-core records: refining and extending the INTIMATE event stratigraphy. Quat. Sci. Rev. 106, 14–28.

Reyes, S., Mejía-Trejo, A., 1991. Tropical perturbations in the eastern Pacific and the precipitation field over north-western Mexico in relation to the ENSO phenomenon. Int. J. Climatol. 11, 515–528.

Rhodes, R.H., Brook, E.J., Chiang, J.C., Blunier, T., Maselli, O.J., McConnell, J.R., Romanini, D., Severinghaus, J.P., 2015. Enhanced tropical methane production in response to iceberg discharge in the North Atlantic. Science 348 (6238), 1016–1019.

Robles, J., Marinone, S., 1987. Seasonal and interannual thermocline variability on the Guaymas Basin in the gulf of California. Continent. Shelf Res. 7, 715–733.

Rodgers, K.B., Blanke, B., Madec, G., Aumont, O., Ciais, P., Dutay, J.C., 2003. Extratropical sources of equatorial Pacific upwelling in an OGCM. Geophys. Res. Lett. 30 (2) https://doi.org/10.1029/2002GL016003.

Rogers, P.J., Johnson, R.H., 2007. Analysis of the 13-14 July gulf surge event during the 2004 North American Monsoon experiment. Mon. Weather Rev. 135, 3098–3117.

Romero, O.E., Leduc, G., Vidal, L., Fischer, G., 2011. Millennial variability and long-term changes of the diatom production in the eastern equatorial Pacific during the last glacial cycle. Paleoceanography 26 (2). https://doi.org/10.1029/2010PA002099.

Rose, D.T., Cox, E.J., 2013. Some diatom species do not show a gradual decrease in cell size as they reproduce. Fundamental and Appled Limnology 182 (2), 117–122.

Routson, C.C., Erb, M.P., McKay, N.P., 2022. High latitude modulation of the Holocene north American monsoon. Geophys. Res. Lett. 49 (16) https://doi.org/10.1029/2022GL099772.

Sancetta, C., 1995. Diatoms in the Gulf of California: seasonal flux patterns and the sediment record for the past 15,000 years. Paleoceanography 10, 67–84.

Sancetta, C., Villareal, T.A., Falkowski, P., 1991. Massive fluxes of rhizosolenid diatoms: a common occurrence? Limnol. Oceanogr. 36, 1452–1457.

Santamaría-del-Angel, E., Alvarez-Borrego, S., Müller-Karger, F.E., 1994. Gulf of California biogeographic regions based on coastal zone color scanner imagery. J. Geophys. Res. 99 (C4), 7411–7421.

Sarmiento, J.L., Gruber, N., Brzezinski, M.A., Dunne, J.P., 2004. High-latitude controls of thermocline nutrients and low latitude biological productivity. Nature 427, 56–60.

Schimmelmann, A., Lange, C.B., Schieber, J., Francus, P., Ojala, A.E.K., Zolitschka, B., 2016. Varves in marine sediments: a review. Earth Sci. Rev. 159, 215–246.

Schrader, H., 1982. Diatom biostratigraphy and laminated diatomaceous sediments from the gulf of California deep sea drilling Project Leg 64. In: Curray, J.R., Moore, D.G., et al. (Eds.), Init. Repts. DSDP. U.S. Govt. Printing Office, Washington, pp. 973–981.

Schrader, H., Kelts, K., Curray, J., Moore, D., Aguayo, E., Aubry, M., Einsele, G., Fornari, D., Gieskes, J., Guerrero, J., Kastner, M., Lyle, M., Matoba, Y., Molina-Cruz, A., Niemitz, J., Rueda, J., Saunders, A., Simoneit, B., Vaquier, V., 1980. Laminated diatomaceous sediments from the Guaymas Basin slope (central Gulf of California): 250,000-year climate record. Science 207, 1207–1209.

Schrader, H., Sorknes, R., 1991. Peruvian coastal upwelling - late Quaternary productivity changes revealed by diatoms. Mar. Geol. 97, 233–249.

Schuette, G., Schrader, H., 1981. Diatom taphocoenoses in the coastal upwelling area off South West Africa. Mar. Micropaleontol. 6, 131–155.

Schulz, M., Mudelsee, M., 2002. REDFIT: estimating red-noise spectra directly from unevenly spaced paleoclimatic time series. Comput. Geosci. 28, 421–426.

Seager, R., Ting, M., Davis, M., Cane, M., Naik, N., Nakamura, J., Li, C., Cook, E., Stahle, D.W., 2009. Mexican drought: an observational modeling and tree ring study of variability and climate change. Atmósfera 22, 1–31.

Seeberg-Elverfeldt, I.A., Lange, C.B., Pätzold, J., 2004a. Preservation of siliceous microplankton in surface sediments of the northern Red Sea. Marine Micropalaeontology 51, 193–211.

Seeberg-Elverfeldt, I.A., Lange, C.B., Arz, H.W., Pätzold, J., Pike, J., 2004b. The significance of diatoms in the formation of laminated sediments of the Shaban Deep, Northern Red Sea. Mar. Geol. 209, 279–301.

Shipboard-Scientific-Party, 1982. Guaymas Basin slope: sites 479 and 480. In: Curray, J. R., Moore, D.G., et al. (Eds.), Initial Reports, DSDP 64. U.S. Govt. Printing Office), Washington, pp. 417–504.

Skakala, J., Bruun, J.T., 2018. A mechanism for Pacific interdecadal resonances. J. Geophys. Res. Oceans 123, 6549–6561.

Soto-Mardones, L., Marinone, S.G., Pares-Sierra, A., 1999. Time and spatial variability of sea surface temperatures in the gulf of California. Cienc. Mar. 25, 1–30.

Stolte, W., Riegman, R., 1996. A model approach for size-selective competition of marine phytoplankton for fluctuating nitrate and ammonium. J. Phycol. 32, 732–740.

Strub, P.T., James, C., 2002. The 1997-1998 oceanic El Niño signal along the southeast and northeast Pacific boundaries–an altimetric view. Prog. Oceanogr. 54, 439–458.

Stuiver, M., Grootes, P.M., 2000. GISP2 oxygen isotope ratios. Quat. Res. 53, 277–283.

Sutton, R.T., Hodson, D.L.R., 2005. Atlantic Ocean forcing of North American and European summer climate. Science 309, 115–118.

Svensson, A., Andersen, K.K., Bigler, M., Clausen, H.B., Dahl-Jensen, D., Davies, S.M., Johnsen, S.J., Muscheler, R., Parrenin, F., Rasmussen, S.O., Roethlisberger, R., Seierstad, I., Steffensen, J.P., Vinther, B.M., 2008. A 60 000 year Greenland stratigraphic ice core chronology. Clim. Past 4, 47–57.

Takahashi, K., Onodera, J., Katsurada, Y., 2009. Relationship between time-series diatom fluxes in the central and western equatorial Pacific and ENSO-associated migrations of the Western Pacific Warm Pool. Deep-Sea Res. I 56, 1298–1318.

Talley, L.D., 1999. Some aspects of ocean heat transport by the shallow, intermediate and deep overturning circulations. In: Clark, P.U., Webb, R.S., Keigwin, L.D. (Eds.), Mechanisms of Global Climate Change at Millenial Time Scales, vol. 112. Wiley, pp. 1–22. American Geophysical Union, Geophysical Monograph Series.

Thunell, R., Pride, C., Tappa, E., Muller-Karger, F., 1993. Varve formation in the Gulf of California: insights from time series sediment trap sampling and remote sensing. Quat. Sci. Rev. 12, 451–464.

Thunell, R.C., 1998. Seasonal and annual variability in particle fluxes in the Gulf of California: a response to climate forcing. Deep-Sea Res. I 45, 2059–2083.

Toggweiler, J.R., Dixon, K., Broecker, W.S., 1991. The Peru upwelling and the ventilation of the south-pacific thermocline. J. Geophys. Res. Oceans 96, 20467–20497.

Tsuchiya, M., Lukas, R., Fine, R.A., Firing, E., Lindstrom, E., 1989. Source waters if the pacific equatorial undercurrent. Prog. Oceanogr. 23, 101–147.

Tudhope, A.W., Chilcott, C.P., McCulloch, M.T., Cook, E.R., Chappell, J., Ellam, R.M., Lea, D.W., Lough, J.M., Shimmield, G.B., 2001. Variability in the El nino - southern oscillation through a glacial-interglacial cycle. Science 291, 1511–1517.

Turney, C.S.M., Kershaw, A.P., Clemens, S.C., Branch, N., Moss, P.T., Fifield, L.K., 2004. Millennial and orbital variations of El Nino/Southern Oscillation and high-latitude climate in the last glacial period. Nature 428, 306–310.

Velázquez-Aguilar, M., Pérez-Cruz, L., Urrutia-Fucugauchi, J., Marsaglia, K.M., Coria-Monter, E., Monreal-Gómez, M.A., Teske, A., Höfig, T.W., Aldama-Cervantes, A., Jiang, S.D., 2024. Evolution of water masases in the Guaymas Basin (Gulf of California) during the last 31,000 years revealed by radiolarians and silicoflagellates in IODP expedition 385 cores. Front. Earth Sci. https://doi.org/10.3389/feart.2024.1301999.

Vera, C., Higgins, W., Amador, J., Ambrizzi, T., Garreaud, R., Gochis, D., Gutzler, D., Lettenmaier, D., Marengo, J., Mechoso, C.R., Nogues-Paegle, J., Dias, P.L.S., Zhang, C., 2006. Toward a unified view of the American Monsoon Systems. J. Clim. 19, 4977–5000.

WAIS Divide Members, 2015. Precise interpolar phasing of abrupt climate change during the last ice age. Nature 520, 661–665.

Wang, R., Nan, F., Yu, F., Wang, B., 2022. Subantarctic mode water variations in the three southern hemisphere ocean basins during 2004-2019. J. Geophys. Res. Oceans 127 (7). https://doi.org/10.1029/2021JC017906.

Warnock, J., Scherer, R., Loubere, P., 2007. A quantitative assessment of diatom dissolution and late quaternary primary productivity in the Eastern Equatorial Pacific. Deep-Sea Research Pt II 54, 772–783.

Weedon, G.P., 2003. Time-Series Analysis and Cyclostratigraphy: Examining Stratigraphic Records of Environmental Cycles. Cambridge University Press, Cambridge.

Yu, J., Anderson, R.F., Jin, Z.D., Ji, X., Thornally, D.J.R., Wu, L., Xie, X., Rohling, E.J., McManus, J.F., 2023. Millennial atmospheric $CO_2$ changes linked to ocean ventilation modes over past 150,000 years. Nat. Geosci. 16, 1166–1173.

Zolotokrylin, A.N., Titkova, T.B., Brito-Castillo, L., 2016. Wet and dry patterns associated with ENSO events in the Sonoran Desert from, 2000-2015. J. Arid Environ. 134, 21–32.

Zuo, H., Naveira-Garabato, A.C., New, A.L., Oschliess, A., 2012. Mechanisms of subantarctic mode water upwelling in a hybrid-coordinate global GCM. Ocean Model. 45–46, 59–80.